Transcription factor TAp73 and microRNA-449 cooperate in multiciliogenesis

Running title: TAp73 and miR449 cooperate in multiciliogenesis

Merit Wildung[1#], Tilman U. Esser[1#], Katie B. Grausam[2,3], Cornelia Wiedwald[1], Li Li[2], Jessica Zylla[2], Ann-Kathrin Guenther[4], Magdalena Wienken[5], Evrim Ercetin[1], Felix Bremmer[6], Orr Shomroni[7], Stefan Andreas[1], Haotian Zhao[2,3,8*] and Muriel Lizé[1,*]

 # = equal contribution; * = corresponding authors

1) **Molecular & Experimental Pneumology Group, Clinic for Cardiology and Pneumology, University Medical Center Goettingen, Germany**
2) **Cancer Biology and Immunotherapeutics Group, Sanford Research, Sioux Falls, South Dakota, USA**
3) **Division of Basic Biomedical Sciences, University of South Dakota, Sanford School of Medicine, Vermillion, South Dakota**
4) **Department of Genes and Behavior, MPI for Biophysical Chemistry, Goettingen, Germany**
5) **Institute of Molecular Oncology, University Medical Center Goettingen, Germany**
6) **Institute of Pathology, University Medical Center Goettingen, Goettingen, Germany**
7) **Microarray and Deep-Sequencing Core Facility, University Medical Center Goettingen, Germany**
8) **Department of Biomedical Sciences, New York Institute of Technology College of Osteopathic Medicine, Old Westbury, New York, USA**

Competing Financial Interest Statement

The authors declare no competing financial interests.

Funding: Our work was supported by the Deutsche Forschungsgemeinschaft, New York Institute of Technology, Sanford Research, Matthew Larson Foundation, Institutional Development Award from the National Institute of General Medical Sciences, National Cancer Institute, Wilhelm-Sander-Stiftung and the Max Planck Society.

Corresponding author: Muriel Lizé: mlize@gwdg.de

Abstract

Motile cilia serve vital functions in development, homeostasis and regeneration. We recently demonstrated that TAp73 is an essential transcriptional regulator of respiratory motile multiciliogenesis. Here, we show that TAp73 is expressed in multiciliated cells (MCCs) of diverse tissues. Analysis of *TAp73*$^{-/-}$ animals revealed that TAp73 regulates *Foxj1*, *Rfx2, Rfx3*, axonemal dyneins *Dnali1* and *Dnai1*, plays a pivotal role in the generation of MCCs in reproductive ducts, and contributes to fertility. However, in the brain the function of MCCs appears to be preserved upon loss of TAp73, and robust activity from cilia-related networks is maintained in *TAp73*$^{-/-}$. Consistent with *TAp73*$^{-/-}$, its target *miR34bc* was reduced, whereas strong and specific induction of *miR449* was observed along with an increase in *E2f4,* that induced transcriptional response from *miR449* genomic regions. Depletion of both *TAp73* and *miR449* resulted in defective multiciliogenesis in the brain and hydrocephalus, indicating that miR449 and potentially additional pro-ciliogenic factors cooperate with TAp73 to ensure brain multiciliogenesis and CP development.

Introduction

Cilia are hair-like appendages protruding from the cell membrane into the surrounding environment. While single immotile primary cilia are a common organelle of most mammalian cells, motile cilia are restricted to a subset of cell types. This subset includes multiciliated cells (MCCs) lining the ventricles of the brain, the tracheal and bronchial epithelium as well as the epithelium of the efferent ducts (EDs) and fallopian tubes (FTs) in the male and female reproductive tract, respectively [1].

Motile multiciliogenesis requires precise regulation of the production, transport and assembly of a large number of different structural components, a process critically dependent on a hierarchical network of transcriptional and posttranscriptional regulators [2]. Geminin Coiled-Coil Domain Containing 1 (GEMC1) [3–5] and multiciliate differentiation and DNA synthesis associated cell cycle protein (MCIDAS or Multicilin) [6–8], members of the Geminin family, are early regulators of the MCC fate, downstream of the NOTCH pathway. Inhibition of the NOTCH pathway e.g. by microRNA-449 (miR449) is required for multiciliogenesis through de-repression of the transcriptional network of *GEMC1*, *MCIDAS*, E2F transcription factors (*E2F4*, *E2F5*), forkhead box J1 (*FOXJ1*), and v-myb avian myeloblastosis viral oncogene homolog (*MYB)* [9,10]. Disturbance of the molecular circuit leads to defective multiciliogenesis and ciliopathies in the airways, reproductive tracts and the brain.

Transformation related protein 73 (*Trp73*) is a member of the p53 family with distinct isoforms generated from two alternative promoters: isoforms containing the N-terminal transactivation domain (TAp73), and N-terminally truncated dominant-negative isoforms (ΔNp73). Recently, we and others showed that TAp73 is essential for airway multiciliogenesis [11,12]. Gene expression analysis and chromatin immunoprecipitation (ChIP) identified TAp73 as a critical regulator of multiciliogenesis: TAp73 acts downstream of E2F4/MCIDAS, and regulates the expression of *FOXJ1*, *RFX2,* and *RFX3* in pulmonary tissues [11,13–16].

The FT of the female reproductive tract can be subdivided in isthmus, the ampulla, and the infundibulum. MCCs within the FTs possess hundreds of motile cilia beating in a wave-like manner which, along with musculature contraction, moves the oocyte or zygote towards the uterus [17–19]. Defects in ciliary functions may lead to ectopic pregnancies or infertility [18,20]. In the male reproductive tract, MCCs in the EDs transport the spermatozoa from testis to epididymis (Epi) [21,22].

MCCs in the brain can be found in a single layer of ependymal cells facing the ventricles and choroid plexus (CP). The CP epithelium, a specialized secretory epithelium that secretes cerebrospinal fluid, arises from monociliated progenitors in the roof plate around embryonic day (E) 12 [23,24]. Ependymal cells in mice are specified around day E16 and form multiple motile cilia on the apical surface after birth to facilitate cerebrospinal fluid movement [25,26]. Defects in the ependymal and CP lineages are implicated in aging, hydrocephalus, and brain tumors [27,28].

In this study, we detected robust TAp73 expression in MCCs in diverse tissues. Consistently, *TAp73* loss leads to a profound reduction of multiciliogenesis in the FTs and EDs and a significant loss of activity in the TAp73-dependent transcriptional network. However, *TAp73* is dispensable for functional MCCs in the brain, which maintains a robust multiciliogenesis program. Molecular studies revealed significant alterations in pro-ciliogenic factors of the *miR-34/449* family in the brain of *TAp73*$^{-/-}$ mice: reduced expression of the TAp73 target *miR34bc* is concurrent with a strong *miR449* induction, suggesting that the increase in *miR449* might partially rescue brain ciliogenesis in the absence of *TAp73*. Indeed, loss of both *TAp73* and *miR449* leads to a dramatic loss of multiciliogenesis in the CP and severe hydrocephalus. Therefore, the molecular network governing multiciliated cell fate is subjected to tissue-specific feedback modulation.

Materials and Methods

Animals

TAp73 mutant mice with targeted deletion of exons 2 and 3 of the *Trp73* gene were a generous gift from Dr. Tak Mak (Princess Margaret Cancer Centre, Toronto, Canada) [29]. *miR449* mutants were previously described [30]. Both strains were maintained in C57Bl/6 background (n8) at the animal facility of the European Neuroscience Institute Göttingen, Germany in full compliance with

institutional guidelines. The study was approved by the Animal Care Committee of the University Medical Centre Goettingen and the authorities of Lower-Saxony under the number 16/2069.

Human samples

Human epididymis samples were procured with informed consent from two patients (42 and 41 years of age, respectively). All experimental procedures were approved and performed in accordance with the requirements set forth by Ethics Committee of the University Medical Centre Goettingen (application number: 18/2/16).

Histology and immunostaining

Paraformaldehyde-fixed, paraffin-embedded tissues were treated with heat-induced epitope retrieval using Rodent Decloaker (RD913 L, Biocare Medical). For immunohistochemistry, endogenous peroxidase activity was quenched with 3% H_2O_2 for 10 min. Tissue sections were blocked with 10% fetal calf serum (FCS) in phosphate buffered saline (PBS) with 0.1% Triton X-100, and subsequently incubated with primary antibodies (List of antibodies in **Table 1**). Biotinylated secondary antibodies were applied for 1 h at room temperature (List of antibodies in **Table 2**), after which avidin enzyme complex and substrate/chromogen were used for color development (Vector laboratories). Stained tissue sections were counterstained with hematoxylin. For immunofluorescence, sections were stained with fluorescently labeled secondary antibodies (List of antibodies in **Table 2**) for 1 h at room temperature. Nuclei were counterstained with DAPI.

Table 1. Primary antibody information.

Antibodies	**Dilution (Application)**	**Company**	**Catalog # [clone]**
Mouse monoclonal anti-Ac-α-TUB	1:1,000 (IF)	Sigma	T6793 [6-11B-1]
Mouse monoclonal anti- ARL13B	1:500 (IF)	NeuroMab	75-287 [N295B/66]
Rabbit polyclonal anti-ARL13B	1:500 (IHC)	Proteintech	17711-1-AP
Mouse monoclonal anti- AQP1	1:1,000 (IHC, IF)	Abcam	ab9566 [1/22]
Rabbit polyclonal anti-AQP1	1:1,000 (IF)	EMD Millipore	AB2219
Rabbit polyclonal anti-β-ACTIN	1:10,000 (WB)	Abcam	ab8227
Rabbit polyclonal anti-Cytokeratins	1:100 (IHC)	Dako	Z0622
Rabbit polyclonal anti-DNAI1	1:500 (IF); 1:700 (WB)	Sigma	HPA021649
Goat polyclonal anti-DNALI1	1:300 (WB)	Santa Cruz	sc-160296
Rabbit polyclonal anti-FOXJ1	1:500 (WB)	Sigma	HPA005714
Mouse monoclonal anti-HSC70	1:20,000 (WB)	Santa Cruz	sc-7298 [B-6]

Rabbit monoclonal anti-KI-67	1:100 (IF)	Abcam	ab16667 [SP6]
Rabbit polyclonal anti-OTX2	1:500 (IHC)	EMD Millipore	AB9566
Rabbit monoclonal anti-P73	1:100 (IF, IHC); 1:300 (WB)	Abcam	ab40658 [EP436Y]
Rabbit polyclonal anti-TTR	1:100 (IHC)	Proteintech	1189-1-AP

Table 2. Secondary antibody information.

Antibodies	**Dilution (Application)**	**Company**	**Catalog #**
Alexa Fluor 488 donkey anti-mouse	1:500 (IF)	Thermo Fisher Scientific	A21202
Alexa Fluor 594 goat anti-rabbit	1:500 (IF)	Thermo Fisher Scientific	A11012
Peroxidase-conjugated donkey anti-mouse	1:10,000 (WB)	Jackson Immunoresearch	715-036-150
Peroxidase-conjugated donkey anti-goat	1:10,000 (WB)	Jackson Immunoresearch	705-036-147

Peroxidase-conjugated donkey anti-rabbit	1:10,000 (WB)	Jackson Immunoresearch	711-036-152
Biotin-SP-conjugated AffiniPure Goat Anti-Rabbit IgG	1:1,000 (IHC)	Jackson ImmunoResearch	111-065-144
Biotin-SP-conjugated AffiniPure Donkey Anti-Mouse	1:1,000 (IHC)	Jackson ImmunoResearch	715-065-151

Quantification of cilia markers

Cilia were quantified using *ImageJ* software [31]. Briefly, the region of interest was selected and a threshold was set to exclude unspecific background signals. The *Analyze Particles* tool was used to measure the area of the ciliary staining. Values were normalized to the length of the epithelia measured.

Western blot

Samples were homogenized in RIPA buffer (20 mM TrisHCl pH 7.5, 150 mM NaCl, 9.5 mM EDTA, 1% Triton X100, 0.1% SDS, 1% sodium desoxycholate) supplemented with urea (2.7 M) and protease inhibitors (Complete Mini EDTA-free, Roche). Equal amounts of protein extracts were separated by SDS-polyacrylamide gels prior to transfer onto a nitrocellulose membrane and incubated with primary antibodies (List of antibodies in **Table 1**). The membrane was washed and incubated for 1 hour with horse radish peroxidase (HRP)-conjugated secondary antibodies (List of antibodies in **Table 2**) followed by chemiluminescence detection. β-ACTIN or heat shock cognate 71 kDa protein (HSC70) were used as protein loading controls.

RNA extraction, quantitative PCR, *in situ* hybridization, and small RNA sequencing

Tissue samples (for the brain: coronal slices with an enrichment of the lateral ventricle were used, blue dotted lines in Fig. 1f indicate the cutting area) were snap-frozen in liquid nitrogen and total RNA was isolated by Extrazol (7BioScience)/Chloroform extraction followed by 80% ethanol precipitation at -20 °C. For cDNA synthesis, 1 µg of total RNA was incubated with the M-MuLV reverse transcriptase and a mix of random nonameric and polyA tail primers at 42 °C for 1 h in a total volume of 50 µl. All reactions were set up in triplicate with self-made SYBR Green qPCR Mix (Tris-HCl [75 mM], (NH4)2SO4 [20 mM], Tween-20 [0.01% v/v], MgCl2 [3 mM], Triton X-100 [0.25% v/v], SYBR Green I (1:40,000), dNTPs [0.2 mM] and Taq-polymerase [20 U/ml]) using 250 nM of each gene-specific primers (List of primers in Table 3). Standard curve method was used to assess relative transcript content. Transcript of interests were normalized to the reference transcript of ribosomal phosphoprotein P0 (Rplp0, or 36b4) and normalized to the mean value of control samples. The results for each sample were obtained by averaging transcript levels of technical triplicates. No RT controls and dilution curves as well as melting curves and gel electrophoresis assessment of amplicons were performed for all primer combinations. For miR-449a quantification, TaqMan MicroRNA Assay (Thermo Fisher Scientific) was performed according to the manufacturer's instructions with U6 snRNA as internal control.

Hes1 (probe no. 417701) and *Hes5* (probe no. 400991-C2) were visualized using RNAscope 2.5 HD Duplex Reagent Kit (#322430, Advanced Cell Diagnostics, Hayward, CA) according to manufacturer's instructions.

The libraries for Small RNA samples were prepared using TruSeq Small RNA Library Prep Kit - Set A (24 rxns) (Set A: indexes 1-12; Cat N°: RS-200-001) using 1 µg of total RNA according to manufacturer's recommendations. Samples were sequenced on the Illumina HiSeq 4000 using a 50 bp single-end approach. Mapping, prediction of novel miRNAs, quality control, and differential

expression (DE) analysis were carried out using Oasis2.0 (*Oasis: online analysis of small RNA deep sequencing data*) [32]. In brief, FASTQ files were trimmed with cutadapt 1.7.1 [33] removing Truseq adapter sequences (TGGAATTCTCGGGTGCCAAGG) followed by removing sequences smaller than 15 or larger than 32 nucleotides. Trimmed FASTQ sequences were aligned to mouse sRNAs using STAR version 2.4.1d [34] with a mismatch of 5% of the sequence length and by utilizing the following databases: Mirbase version 21 for microRNA (miRNAs); piRNAbank V.2 for piwiRNA (piRNA); and Ensembl v84 for small nuclear RNA (snRNA), small nucleolar RNA (snoRNA) and ribosomal RNA (rRNA). Counts per small RNA were calculated using featureCounts v1.4.6 [35]. Novel miRNAs were searched for using miRDeep2 version 2.0.0.5 [36]. Differential expression of small RNA was determined by DESeq2 [37], where sRNAs were considered differentially expressed with an adjusted p-value <0.05 and absolute log2 fold-change >1. The results of the DE analysis can be found in **Supplementary Table S1**, and the sRNA-seq data sets can be found in Gene Expression Omnibus (GEO) with accession number **GSE108385**.

Table 3. Sequence information for primers used in RT-qPCR.

Gene	Accession number	Amplicon bp	Exons	Forward primer	Reverse primer
TAp73	NM_011642	163	Ex2-Ex3	5'-AGCAGAATGAGCGGCAGCGTT-3'	5'-TGTTGGACTCCTCGCTGCCTGA-3'
Foxj1	NM_008240	200	Ex2-Ex3	5'-CCATGCAGACCCCACCTGGCA-3'	5'-GGGCAAAGGCAGGGTGGATGT-3'

Dnali1	NM_175223	213	Ex4-Ex5	5'-TTTGGCATGAGGAAGGCACT-3'	5'-CTGGTTGGTCCGTTTCAGGA-3'
Mcidas	NM_001037914	137	Ex7	5'-AACAACGAAAAGGAGCCTGGA-3'	5'-GCCGCTTAGGGTCACGATTG-3'
E2f4	NM_148952	199	Ex7-Ex9	5'-GCACTGGACACTCGGCCT-3'	5'-TGCACTCTCTCGTGGGGTCG-3'
Rfx2	NM_027787	74	Ex5-Ex6	5'-GACGGCACAAGACACTCTCTG-3'	5'-AGAGTCTCAATCGCCATTTCAAG-3'
Rfx3	NM_001360357	107	Ex3	5'-ATGCAGACTTCAGAGACGGGT-3'	5'-ACTGGCACTTGCTGTACCAC-3'
36b4	NM_007475	155	Ex6-Ex7	5'-GCAGATCGGGTACCCAAC-3'	5'-CAGCAGCCGCAAATGCAG-3'

Chromatin immuno-precipitation (ChIP)

Chromatin was harvested from Saos2 cells transiently overexpressing TAp73α, TAp73β and the control vector pcDNA3.1. ChIP and qPCR was performed as previously described using gene specific primers (List of primers in **Table 4**) [11]. Enrichment levels were determined as the number of PCR products for each gene relative to total input.

Table 4. Sequence information for primers used in ChIP-qPCR.

Gene	Forward primer	Reverse primer
FOXJ1 down	5'-CAGCATGCCCAGAAGCTTTG-3'	5'-TCAGGGGCTGCATTCTTCC-3'
FOXJ1 end	5'-AGGGCACACTTAGCCTTTG-3'	5'-AGGAGACAAAGGGAGGAGG-3'
DNAI1	5'-CCCAAGCGGGGTAATCTCT-3'	5'-CTTGAGGTTGTGGGACTTCAC-3'
DNALI1	5'-CACGCCCGGCAAATTTCTG-3'	5'-CAAGGTGGGCAGATCATGTG-3'

Luciferase assay

Luciferase assay was performed as previously described [11]. Briefly, Saos2 cells were transfected with pcDNA3.1 empty vector, or pcDNA3.1 vector carrying *E2F4* or MCIDAS, or both *E2F4* and *MCIDAS* vectors. Moreover, a firefly luciferase reporter construct containing the putative three wild type E2F-binding sequence of *miR449* genomic region (wild type, or "WT"), or the same sequence lacking the strongest predicted E2F-binding motif (mutant, or "Mut") were transfected (**Table 5**). In addition, a Renilla TK luciferase vector was co-transfected. At 24 h after transfection, cells were harvested and the luciferase activities were measured using the dual luciferase assay. Firefly luciferase activities were determined relative to those of Renilla TK luciferase vector and normalized to the mean value of samples from the control vector.

Table 5: Luciferase constructs for E2F4/MCIDAS luciferase reporter assay.

RS: Restriction site

Construct name	**DNA sequence of inserts** The strongest E2F binding site is depicted in grey and the removed sequence in **bold underlined**. Two consensus sequences with lower score were retained in the mutant (pink and red).	**Vector**	**5' RS**	**3' RS**
miR449/Cdc20b WT E2F binding site = **WT**	GCCAGAAAGCTGAGCACACTGGGGACT CCGTGATAAAGGGGGAGAGGAAGATAT TGAGGGTTGAGGAAGAGGTCTG**GCGGG** **AAAT**GACAGGGAACCAGATGGGCTGTG CAGCCTTAGCTGCCCATCTGAGCTGCC AAGAGAGCCGAGTTGTGCCATATGGCA GGAG	pGL4.23	NheI	EcoRV
miR449/Cdc20b Mut E2F binding site = **Mut**	GCCAGAAAGCTGAGCACACTGGGGACT CCGTGATAAAGGGGGAGAGGAAGATAT TGAGGGTTGAGGAAGAGGTCTGGACAG GGAACCAGATGGGCTGTGCAGCCTTAG CTGCCCATCTGAGCTGCCAAGAGAGCC GAGTTGTGCCATATGGCAGGAG	pGL4.23	NheI	EcoRV

Video microscopy

Murine fallopian tube and testis connected to the epididymis were dissected and transferred to Dulbecco's Modified Eagle's Medium (DMEM, Thermo Fisher Scientific). To image spermatocytes, the epididymis was separated from testis and vas deferens. An incision was made at distal end to release to spermatocytes. Spermatocytes as well as the peristaltic contraction of the fallopian tube was imaged with an inverse microscope.

Imaging of cilia-generated bead-flow and cilia beating in the brain ventricular system

Mouse brains were dissected and transferred to DMEM 21063 (Thermo Fisher Scientific). Lateral ventricle (LV) and ventral third ventricle (v3V) were prepared from a 1 mm coronal slice, a 3 mm slice, and two 1 mm slices in a coronal adult brain matrix (ASI Instruments) as previously described [38]. Tissue explant was placed in DMEM containing fluorescent latex beads (Fluoresbrite Multifluorescent 1.0 micron Microspheres, Polysciences). Movement of fluorescent beads along the ventricular wall and within ventricular lumen was observed by fluorescence microscopy using a DMR (Leica) upright microscope with an epifluorescence lamp. Ciliary beating was observed by differential interference contrast (DIC) microscopy using the same set-up. Bead movement was recorded using a high-speed camera operated by MultiRecorder Software (Cascade II-512, Photometrics) and analysed using ImageJ software [31].

Statistical Analysis

One-tailed, unpaired Student's test assuming normal distribution was used to calculate statistical significance for pairwise comparisons. Luciferase assay statistics were assessed using one-way ANOVA assuming normal distribution followed by Dunnett's multiple comparison tests. The following indications of significance were used: $*P<0.05$, $**$ $P<0.01$, $***$ $P<0.001$. N values represent biological replicates. Error bars indicate standard error of the mean (SEM).

Results

TAp73 is expressed in diverse multiciliated epithelia in development and adulthood

We and others previously showed that TAp73 expressed in respiratory epithelia controls multiciliogenesis [11,12]. However, little is known about the expression and function of TAp73 in other multiciliated cell types. To this end, quantitative PCR with reverse transcription (RT-qPCR) revealed abundant *TAp73* mRNA in ciliated tissues including efferent ducts (EDs), fallopian tubes (FTs), and brain ventricles/choroid plexus (CP), in addition to the testis as previously described [39,40] (**Fig. 1a**). In humans, we identified nuclear localization of P73 in FTs and EDs (**Fig. 1b-e**). In mice, TAp73 expression was detected in ependymal and CP epithelial cells (**Fig. 1f and g**). During development, proliferative progenitors (KI-67^{+}) are present in hindbrain roof plate, whereas post-mitotic cells expressing Aquaporin 1 (AQP1) [28,41] are detected in CP epithelium (KI-67^{-}/AQP1^{+}) (**Fig. 1h**). Notably, a portion of the roof plate exists between the progenitors and CP epithelium that remains undifferentiated after cell cycle exit (KI-67^{-}/AQP1^{-}) (**Fig. 1h**). In contrast to progenitors with a solitary primary cilium, the “transition” zone is comprised of MCCs that exhibit P73 expression at day E14.5 (**Fig. 1i**). Altogether, these data suggest a role for TAp73 in multiciliogenesis in reproductive tracts and the brain.

TAp73 is crucial for the molecular circuit of multiciliogenesis in efferent ducts

Loss of *TAp73* leads to male infertility that has been attributed to defective spermatocyte production [39,40]. However, flagellated and motile spermatocytes are present in *TAp73*$^{-/-}$ mice, though at markedly reduced levels (**Fig. 2a; Supplementary Video S1a-d**), suggesting that additional defects as a result of *TAp73* loss may contribute to infertility in these mice. The multiciliated epithelium of the ED is involved in gamete transport from the testis to the epididymis,

sperm concentration, and maturation [21,42], all essential aspects of male fertility [43]. Indeed, though no gross morphological differences were observed in EDs between control and *TAp73* knockout (KO) animals (**Fig. 2b**), staining of the cilia components acetylated alpha-tubulin (Ac-α-TUB) and axonemal dynein DNAI1 revealed a dramatic reduction in the number and length of cilia in the EDs of mutant mice (**Fig. 2c and d**), resembling the loss of airway cilia in these mice. ChIP followed by quantitative PCR (ChIP-qPCR) revealed significant enrichment of TAp73 in genomic loci of *FOXJ1* and the axonemal dyneins *DNALI1* and *DNAI1* (**Fig. 2e;** ChIPseq track depicted in **Supplementary Fig. S1**). Accordingly, protein products of DNAI1 and DNALI1 and transcript products of *Dnali1*, *Foxj1*, *Rfx2,* and *Rfx3* were reduced or almost completely lost in male reproductive ducts of *TAp73* KO animals (**Fig. 2f, g and h**, respectively). Together, our results indicate that TAp73 directs *Dnali1* and *Dnai1* in addition to known critical nodes including *Foxj1*, *Rfx2,* and Rfx*3* in EDs (**Fig. 6a and b**).

TAp73-driven network of transcription factors regulates multiciliogenesis in fallopian tubes

Though female infertility is associated with the loss of *TAp73,* it is thought to arise from the failure of oocyte release from the ovary and oocyte progression along the FTs [29] (**Fig. 1b**), it remains unclear how *TAp73* loss affects the gamete transport. To address this, we examined the FTs of *TAp73* KO animals and found a profound reduction in cilia coverage in the oviduct epithelium despite normal tubal morphology (**Fig. 3a and b**). Similar to observations in *TAp73*$^{-/-}$ EDs, protein products of genes bound by TAp73 (**Fig. 2e**) such as FOXJ1, DNAI1 and DNALI1 (all expressed in the human FTs, cf. **Supplementary Fig. S2**) and transcript products of *Dnali1*, *Foxj1*, *Rfx2,* and *Rfx3* were significantly reduced in *TAp73*$^{-/-}$ FTs (**Fig. 3c and 3d,** respectively). However, the loss of the TAp73-driven multiciliogenesis program in FTs was not as profound as in EDs. Further, evaluation of the smooth muscle contraction pattern in FTs revealed no difference between

control and *TAp73* KO animals (**Supplementary Video S2a and b**). Therefore, these data indicate that loss of TAp73 leads to reduced multiciliogenesis in the oviduct that may cause defective oocyte transport [29] (**Fig. 6c**).

Ciliary function in the brain is unaltered in the absence of *TAp73*

The expression of TAp73 in ependymal and CP epithelial cells (**Fig. 1a, g and i**), along with recent studies suggesting the role of MCIDAS/E2F4 in multiciliogenesis of these cells [7,44,45], led us to examine the role of *TAp73* in MCCs in the brain. Morphological and gene expression studies revealed no apparent defect in ependymal cells and the CP in *TAp73* KO brains and confirmed lack of P73 expression (**Fig. 4a and b**). We performed immunostainings for the cilia markers Ac-α-TUB, DNAI1, and ADP-ribosylation factor-like 13b (ARL13B; [46]) in the lateral and 4th ventricle. In contrast to FTs and EDs, our results showed that the number and length of cilia from ependymal and CP cells in *TAp73*$^{-/-}$ animals are similar to those of control animals (**Fig. 4c and e; Supplementary Fig. S3a and b**). Consistently, ciliary beating and bead flow in cerebrospinal fluid appeared unaffected by *TAp73* KO (**Fig. 4d; Supplementary Video S3a and b**). Furthermore, no significant difference was observed in the expression of markers for epithelial differentiation of CP between control and *TAp73*$^{-/-}$ animals (**Supplementary Fig. S3c-f**). RT-qPCR analysis demonstrated comparable expression of *Dnali1* and *Foxj1,* whereas increased *Rfx2* and *Rfx3* mRNA levels were observed in brain ventricles of *TAp73* KO mice (**Fig. 4f**). Taken together, these results indicate that the function of MMCs in the brain remains intact despite the loss of *TAp73* (**Fig. 6d**).

TAp73 functions through posttranscriptional codes in brain multiciliogenesis

Besides transcription factors, TAp73 utilizes posttranscriptional mechanisms involving micro RNAs. Consistently, sequencing of small RNA species from brain ventricles revealed significant reduction in *miR34bc* (**Fig. 5a;** complete small RNA sequencing results in **Supplementary Table S1** and in GEO under accession number **GSE108385**), reminiscent of findings in *TAp73*$^{-/-}$ airways. Remarkably, our analysis also showed a strong induction of the *miR449* cluster (**Fig. 5a; Supplementary Table S1; GSE108385**) that together with *miR34bc* regulates multiciliogenesis in different tissues across species [30,47–49]. In agreement with this, *miR449* is predominantly expressed in the CP and increases significantly by over 10-fold upon *TAp73* loss in ventricles (**Fig. 5b and c**), but not in FT nor ED preparations (**Supplementary Fig. S4**) [50].

miR449 is known to suppress the NOTCH pathway, thereby activating the transcriptional cascade involving MCIDAS/E2Fs [3,6,8,44,48]. Though only a slight and non-significant increase in the transcript levels of *Mcidas* were observed, the expression of *E2f4* in brain ventricles was significantly increased in *TAp73* KO mice compared to control animals (**Fig. 5c**). Previous reports showed that *miR449* can be activated by E2F1 [51,52]. Given the conserved binding motif of the E2F transcription factors, we isolated the genomic region of *miR449* (*miR449* is embedded in *CDC20B* gene) containing putative E2F binding sites to assess interaction with MCIDAS/E2F4 in a luciferase reporter assay. Indeed, *MCIDAS* in combination with *E2F4* elicited a strong transcriptional response from the *miR449* locus, a reaction strongly reduced by mutating the strongest of the three putative E2F binding sites (**Fig. 5d; materials and methods Table 5**). This suggests that increased MCIDAS/E2F4 activity stimulates *miR449* expression in *TAp73* KO brain ventricles.

Our data suggests that the crosstalk between MCIDAS/E2F4 and miR449 may partially compensate for *TAp73* loss in brain multiciliogenesis. To address this, we additionally deleted the *miR449* cluster in the *TAp73* mutant background. Strikingly, *TAp73*$^{-/-}$*xmiR449*$^{-/-}$ (aka *TAp73xmiR449* KO) mice developed severe hydrocephalus (**Fig. 5e; Supplementary Fig. S5a**). Analysis of ARL13B expression revealed that, though *miR449* loss alone resulted in a significant decrease in the length of cilia in CP epithelial, a more pronounced reduction in cilia was observed in *TAp73xmiR449* KO mice (**Fig. 5f and g; Supplementary Fig. S5b**). No significant difference was observed in the expression of genes normally found in CP epithelial cells among wild type, *TAp73* KO, *miR449* KO, and *TAp73xmiR449* KO animals (**Supplementary Fig. S5c-e**). Despite the role of NOTCH signaling in CP development and tumorigenesis [28,53], RNAscope studies revealed similar expression of NOTCH pathway targets *Hes1* and *Hes5* in the roof plate of control, *miR449*$^{-/-}$ and *TAp73xmiR449* KO embryos at day E14.5 (**Supplementary Fig. S6**), indicating normal NOTCH pathway activity in the absence of *miR449*. Together, our data indicate that TAp73 utilizes the unique topology of its transcriptional network to communicate with the *miR-34/449* family and other crucial regulators of motile multiciliogenesis e.g. *E2F4/MCIDAS* to regulate brain ciliogenesis (**Fig. 6 e**).

Discussion

TAp73 activates a plethora of ciliogenic effectors to drive multiciliogenesis in the airways [11,12]. The current study examines the role of TAp73-driven molecular circuit in MCCs of reproductive tracts and the brain. Our results revealed profound changes in both male and female reproductive tracts lacking *TAp73*, suggesting that infertility associated with TAp73 loss can be in part explained by cilia loss. The striking reduction in MCCs in *TAp73*$^{-/-}$ FTs and EDs, together with a diminished *Foxj1*, *Rfx2, and Rfx3* expression, is reminiscent of findings in respiratory epithelia of *TAp73* KO mice. The expression of the dyneins *Dnai1* and *Dnali1*, both of which exhibit TAp73 binding in

their genomic loci, is significantly reduced in mutant animals, indicating that they are part of the TAp73-directed multiciliogenesis program in reproductive tracts.

In *TAp73*$^{-/-}$ males, consistent with previous reports, we found partial degradation of the germinal epithelium and reduced sperm cell production [39,40]. However, although reduced in number, spermatocytes in *TAp73* KO are morphologically normal with beating flagella, raising questions about the underlying causes of sterility in these mice. The efferent ducts connecting testis and epididymis comprise multiciliated cells that are required for the transport of spermatozoa to their storage and maturation location. Our present work reveals that male sterility in mice with defective multiciliogenesis e.g. *TAp73*$^{-/-}$ mice can at least partially be attributed to defective ED epithelia. Hence, the integrity of MCCs is critical for reproductive health.

Disruption of transcriptional regulators of multiciliogenesis consistently leads to infertility in mice and humans [3,54], while fertility issues have been reported in female primary ciliary dyskinesia patients [19,20]. Importantly, *TAp73* is downregulated as women age [55], whereas certain single nucleotide polymorphisms in *TP73* are associated with female patients over 35 years of age seeking *in vitro* fertilization treatment [56,57]. However, further studies using tissue-specific deletion of *TAp73* are necessary to delineate its role in reproductive motile cilia maintenance and fertility.

During embryogenesis, robust *TAp73* expression is initiated at the onset of multiciliated differentiation of ependymal and CP epithelial cells. However, our data indicate that the generation of beating multiciliated cells in the brain appears independent of *TAp73*, although we cannot exclude that *TAp73* KO generates more subtle defects such as in polarity and cilia orientation. In contrast to the dynamic TAp73-dependent program in the airways and reproductive tracts, the expression of *Foxj1, Rfx2*, *and Rfx3* in the *TAp73*$^{-/-}$ brain remains unaltered and exhibits

a slight increase, respectively, suggesting that other effectors maintain the molecular circuit to support MCCs.

Previous studies revealed robust expression of *GemC1* and *E2f/Mcidas*, all of which are capable of transcriptional activation of *Foxj1*, *TAp73* itself, and many other ciliogenic effectors e.g. *Rfx2* and *Rfx3* in MCCs of the brain [4,6,8,44,58]. Indeed, E2F4/MCIDAS activity is induced in response to *TAp73* loss, and therefore may facilitate brain multiciliogenesis in the absence of *TAp73*. In agreement, loss of either *MCIDAS* or *GemC1* leads to defect in MCC differentiation and hydrocephalus [3,6].

Although it is less clear how TAp73 loss results in enhanced MCIDAS/E2F activity, a quick look downstream of TAp73 provides some clues: a decrease of the TAp73 target *mir34bc* is accompanied by an increase in *miR449* in the absence of TAp73. *miR449* induction is commonly observed in *miR34*-deficient MCCs, whereby ablation of the entire *miR-34/449* family impairs multiciliogenesis [30,59]. *miR449* is also known to inhibit the NOTCH pathway to relieve the suppression of multiciliogenesis; however, NOTCH pathway activity in the CP remains unchanged after *miR449* loss. Given the diverse targets of the *miR-34/449* family, it is plausible that *miR449* may enhance MCIDAS/E2F activity independent of NOTCH inhibition. Conversely, transcriptional activation of *miR449* by MCIDAS/E2F complexes may complete the feedback loop to keep the molecular circuit fully engaged in the absence of TAp73.

This interpretation posits that the crosstalk between *miR449* and MCIDAS/E2F serves as a crucial backup for TAp73-driven circuitry in the brain. Indeed, depletion of *miR449* in the absence of *TAp73* results in defective ciliogenesis, indicating that TAp73 functions through miR-34/449 family to generate MCCs in the brain. Of note, complete loss of miR-34/449 family does not recapitulate the hydrocephalus phenotype observed in mice lacking both *TAp73* and *miR449* [30,60]. In addition,

hydrocephalus and secondary cilia depletion were described for *p73* KO mice lacking all isoforms, but were not observed in *TAp73* mutant animals, suggesting a potential role for *ΔNp73* isoforms [61,62]. Taken together, the molecular interactome of the p73 family in brain ciliogenesis is fascinatingly complex and just beginning to unravel.

Acknowledgments

We thank Tak Mak for providing *TAp73* KO mice, Gerd Hasenfuss for support, Matthias Dobbelstein for hosting and Karola Metze, Verena Siol and Sabine Bolte for assistance. M.L. is supported by Deutsche Forschungsgemeinschaft (DFG Li 2405); H.Z. by New York Institute of Technology, Sanford Research, Matthew Larson Foundation, Institutional Development Award from the National Institute of General Medical Sciences under grant numbers 5P20GM103548, 1P20GM103620-01A1, and National Cancer Institute (R01CA220551); F.B. by Wilhelm-Sander-Stiftung (2016.041.1); A.K.G by the Max Planck Society. We thank Heymut Omran's group for introduction to cilia microscopy and Travis Stracker for disclosure of non-published data.

Author Contributions

Me.W. and T.E. characterized cilia defects and gene expression and generated figures. Me.W. and Ma.W. validated TAp73 targets by WB and ChIP. E.E. and F.B. contributed IF analysis of human epididymis. C.W. maintained mice, performed RNA isolation and qPCRs. K.B.G., J.Z., L.L. and H.Z. contributed brain analyzes. O.S. analyzed small RNA sequencing data. S.A. contributed to interpretation and supported the group. M.L. developed the project, interpreted the data, designed and coordinated the experiments to complete this study. Me.W., T.E., H.Z. and M.L. were major contributors to manuscript preparation.

Competing Financial Interest Statement

The authors declare no competing financial interests.

References

1 Spassky N, Meunier A. The development and functions of multiciliated epithelia. *Nat Rev Mol Cell Biol* 2017; **18**: 423–436.

2 Choksi SP, Lauter G, Swoboda P, Roy S. Switching on cilia: transcriptional networks regulating ciliogenesis. *Dev Camb Engl* 2014; **141**: 1427–1441.

3 Terré B, Piergiovanni G, Segura-Bayona S, Gil-Gómez G, Youssef SA, Attolini CS-O *et al.* GEMC1 is a critical regulator of multiciliated cell differentiation. *EMBO J* 2016; **35**: 942–960.

4 Arbi M, Pefani D-E, Kyrousi C, Lalioti M-E, Kalogeropoulou A, Papanastasiou AD *et al.* GemC1 controls multiciliogenesis in the airway epithelium. *EMBO Rep* 2016; **17**: 400–413.

5 Zhou F, Narasimhan V, Shboul M, Chong YL, Reversade B, Roy S. Gmnc Is a Master Regulator of the Multiciliated Cell Differentiation Program. *Curr Biol* 2015; **25**: 3267–3273.

6 Boon M, Wallmeier J, Ma L, Loges NT, Jaspers M, Olbrich H *et al.* MCIDAS mutations result in a mucociliary clearance disorder with reduced generation of multiple motile cilia. *Nat Commun* 2014; **5**: 4418.

7 Ma L, Quigley I, Omran H, Kintner C. Multicilin drives centriole biogenesis via E2f proteins. *Genes Dev* 2014; **28**: 1461–1471.

8 Stubbs JL, Vladar EK, Axelrod JD, Kintner C. Multicilin promotes centriole assembly and ciliogenesis during multiciliate cell differentiation. *Nat Cell Biol* 2012; **14**: 140–147.

9 Danielian PS, Hess RA, Lees JA. E2f4 and E2f5 are essential for the development of the male reproductive system. *Cell Cycle Georget Tex* 2016; **15**: 250–260.

10 Danielian PS, Bender Kim CF, Caron AM, Vasile E, Bronson RT, Lees JA. E2f4 is required for normal development of the airway epithelium. *Dev Biol* 2007; **305**: 564–576.

11 Nemajerova A, Kramer D, Siller SS, Herr C, Shomroni O, Pena T *et al.* TAp73 is a central transcriptional regulator of airway multiciliogenesis. *Genes Dev* 2016; **30**: 1300–1312.

12 Marshall CB, Mays DJ, Beeler JS, Rosenbluth JM, Boyd KL, Santos Guasch GL *et al.* p73 Is Required for Multiciliogenesis and Regulates the Foxj1-Associated Gene Network. *Cell Rep* 2016; **14**: 2289–2300.

13 Blatt EN, Yan XH, Wuerffel MK, Hamilos DL, Brody SL. Forkhead transcription factor HFH-4 expression is temporally related to ciliogenesis. *Am J Respir Cell Mol Biol* 1999; **21**: 168–176.

14 Brody SL, Yan XH, Wuerffel MK, Song SK, Shapiro SD. Ciliogenesis and left-right axis defects in forkhead factor HFH-4-null mice. *Am J Respir Cell Mol Biol* 2000; **23**: 45–51.

15 Chen J, Knowles HJ, Hebert JL, Hackett BP. Mutation of the mouse hepatocyte nuclear factor/forkhead homologue 4 gene results in an absence of cilia and random left-right asymmetry. *J Clin Invest* 1998; **102**: 1077–1082.

16 Yu X, Ng CP, Habacher H, Roy S. Foxj1 transcription factors are master regulators of the motile ciliogenic program. *Nat Genet* 2008; **40**: 1445–1453.

17 Crow J, Amso NN, Lewin J, Shaw RW. Morphology and ultrastructure of fallopian tube epithelium at different stages of the menstrual cycle and menopause. *Hum Reprod Oxf Engl* 1994; **9**: 2224–2233.

18 Lyons RA, Saridogan E, Djahanbakhch O. The reproductive significance of human Fallopian tube cilia. *Hum Reprod Update* 2006; **12**: 363–372.

19 Raidt J, Werner C, Menchen T, Dougherty GW, Olbrich H, Loges NT *et al.* Ciliary function and motor protein composition of human fallopian tubes. *Hum Reprod Oxf Engl* 2015; **30**: 2871–2880.

20 Vanaken GJ, Bassinet L, Boon M, Mani R, Honoré I, Papon J-F *et al.* Infertility in an adult cohort with primary ciliary dyskinesia: phenotype–gene association. *Eur Respir J* 2017; **50**: 1700314.

21 Ilio KY, Hess RA. Structure and function of the ductuli efferentes: a review. *Microsc Res Tech* 1994; **29**: 432–467.

22 Lambot M-AH, Mendive F, Laurent P, Van Schoore G, Noël J-C, Vanderhaeghen P *et al.* Three-dimensional reconstruction of efferent ducts in wild-type and Lgr4 knock-out mice. *Anat Rec Hoboken NJ 2007* 2009; **292**: 595–603.

23 Lun MP, Johnson MB, Broadbelt KG, Watanabe M, Kang Y -j., Chau KF *et al.* Spatially Heterogeneous Choroid Plexus Transcriptomes Encode Positional Identity and Contribute to Regional CSF Production. *J Neurosci* 2015; **35**: 4903–4916.

24 Silva-Vargas V, Maldonado-Soto A, Mizrak D, Codega P, Doetsch F. Age-Dependent Niche Signals from the Choroid Plexus Regulate Adult Neural Stem Cells. *Cell Stem Cell* 2016; **19**: 643–652.

25 Spassky N, Merkle FT, Flames N, Tramontin AD, García-Verdugo JM, Alvarez-Buylla A. Adult ependymal cells are postmitotic and are derived from radial glial cells during embryogenesis. *J Neurosci Off J Soc Neurosci* 2005; **25**: 10–18.

26 Lun MP, Monuki ES, Lehtinen MK. Development and functions of the choroid plexus-cerebrospinal fluid system. *Nat Rev Neurosci* 2015; **16**: 445–457.

27 Del Bigio MR. Ependymal cells: biology and pathology. *Acta Neuropathol (Berl)* 2010; **119**: 55–73.

28 Li L, Grausam KB, Wang J, Lun MP, Ohli J, Lidov HGW *et al.* Sonic Hedgehog promotes proliferation of Notch-dependent monociliated choroid plexus tumour cells. *Nat Cell Biol* 2016; **18**: 418–430.

29 Tomasini R, Tsuchihara K, Wilhelm M, Fujitani M, Rufini A, Cheung CC *et al.* TAp73 knockout shows genomic instability with infertility and tumor suppressor functions. *Genes Dev* 2008; **22**: 2677–2691.

30 Song R, Walentek P, Sponer N, Klimke A, Lee JS, Dixon G *et al.* miR-34/449 miRNAs are required for motile ciliogenesis by repressing cp110. *Nature* 2014; **510**: 115–120.

31 Schindelin J, Arganda-Carreras I, Frise E, Kaynig V, Longair M, Pietzsch T *et al.* Fiji: an open-source platform for biological-image analysis. *Nat Methods* 2012; **9**: 676–682.

32 Capece V, Garcia Vizcaino JC, Vidal R, Rahman R-U, Pena Centeno T, Shomroni O *et al.* Oasis: online analysis of small RNA deep sequencing data. *Bioinformatics* 2015; **31**: 2205–2207.

33 Martin M. Cutadapt removes adapter sequences from high-throughput sequencing reads. *EMBnet.journal* 2011; **17**: 10.

34 Dobin A, Davis CA, Schlesinger F, Drenkow J, Zaleski C, Jha S *et al.* STAR: ultrafast universal RNA-seq aligner. *Bioinforma Oxf Engl* 2013; **29**: 15–21.

35 Liao Y, Smyth GK, Shi W. featureCounts: an efficient general purpose program for assigning sequence reads to genomic features. *Bioinforma Oxf Engl* 2014; **30**: 923–930.

36 Friedländer MR, Mackowiak SD, Li N, Chen W, Rajewsky N. miRDeep2 accurately identifies known and hundreds of novel microRNA genes in seven animal clades. *Nucleic Acids Res* 2012; **40**: 37–52.

37 Love MI, Huber W, Anders S. Moderated estimation of fold change and dispersion for RNA-seq data with DESeq2. *Genome Biol* 2014; **15**: 550.

38 Faubel R, Westendorf C, Bodenschatz E, Eichele G. Cilia-based flow network in the brain ventricles. *Science* 2016; **353**: 176–178.

39 Holembowski L, Kramer D, Riedel D, Sordella R, Nemajerova A, Dobbelstein M *et al.* TAp73 is essential for germ cell adhesion and maturation in testis. *J Cell Biol* 2014; **204**: 1173–1190.

40 Inoue S, Tomasini R, Rufini A, Elia AJ, Agostini M, Amelio I *et al.* TAp73 is required for spermatogenesis and the maintenance of male fertility. *Proc Natl Acad Sci* 2014; **111**: 1843–1848.

41 Huang X, Ketova T, Fleming JT, Wang H, Dey SK, Litingtung Y *et al.* Sonic hedgehog signaling regulates a novel epithelial progenitor domain of the hindbrain choroid plexus. *Dev Camb Engl* 2009; **136**: 2535–2543.

42 Hess RA. The Efferent Ductules: Structure and Functions. In: Robaire B, Hinton BT (eds). *The Epididymis: From Molecules to Clinical Practice*. Springer US: Boston, MA, 2002, pp 49–80.

43 Dacheux J-L, Dacheux F. New insights into epididymal function in relation to sperm maturation. *Reproduction* 2013; **147**: R27–R42.

44 Kyrousi C, Lalioti M-E, Skavatsou E, Lygerou Z, Taraviras S. Mcidas and GemC1/Lynkeas specify embryonic radial glial cells. *Neurogenesis* 2016; **3**: e1172747.

45 Mori M, Hazan R, Danielian PS, Mahoney JE, Li H, Lu J *et al.* Cytoplasmic E2f4 forms organizing centres for initiation of centriole amplification during multiciliogenesis. *Nat Commun* 2017; **8**: 15857.

46 Caspary T, Larkins CE, Anderson KV. The Graded Response to Sonic Hedgehog Depends on Cilia Architecture. *Dev Cell* 2007; **12**: 767–778.

47 Lizé M, Herr C, Klimke A, Bals R, Dobbelstein M. MicroRNA-449a levels increase by several orders of magnitude during mucociliary differentiation of airway epithelia. *Cell Cycle Georget Tex* 2010; **9**: 4579–4583.

48 Marcet B, Chevalier B, Luxardi G, Coraux C, Zaragosi L-E, Cibois M *et al.* Control of vertebrate multiciliogenesis by miR-449 through direct repression of the Delta/Notch pathway. *Nat Cell Biol* 2011; **13**: 693–699.

49 Marcet B, Chevalier B, Coraux C, Kodjabachian L, Barbry P. MicroRNA-based silencing of Delta/Notch signaling promotes multiple cilia formation. *Cell Cycle* 2011; **10**: 2858–2864.

50 Redshaw N, Wheeler G, Hajihosseini MK, Dalmay T. microRNA-449 is a putative regulator of choroid plexus development and function. *Brain Res* 2009; **1250**: 20–26.

51 Lizé M, Pilarski S, Dobbelstein M. E2F1-inducible microRNA 449a/b suppresses cell proliferation and promotes apoptosis. *Cell Death Differ* 2010; **17**: 452–458.

52 Yang X, Feng M, Jiang X, Wu Z, Li Z, Aau M *et al.* miR-449a and miR-449b are direct transcriptional targets of E2F1 and negatively regulate pRb-E2F1 activity through a feedback loop by targeting CDK6 and CDC25A. *Genes Dev* 2009; **23**: 2388–2393.

53 Bill BR, Balciunas D, McCarra JA, Young ED, Xiong T, Spahn AM *et al.* Development and Notch Signaling Requirements of the Zebrafish Choroid Plexus. *PLoS ONE* 2008; **3**: e3114.

54 Amirav I, Wallmeier J, Loges NT, Menchen T, Pennekamp P, Mussaffi H *et al.* Systematic Analysis of CCNO Variants in a Defined Population: Implications for Clinical Phenotype and Differential Diagnosis. *Hum Mutat* 2016; **37**: 396–405.

55 Guglielmino MR, Santonocito M, Vento M, Ragusa M, Barbagallo D, Borzì P *et al.* TAp73 is downregulated in oocytes from women of advanced reproductive age. *Cell Cycle Georget Tex* 2011; **10**: 3253–3256.

56 Hu W, Zheng T, Wang J. Regulation of Fertility by the p53 Family Members. *Genes Cancer* 2011; **2**: 420–430.

57 Feng Z, Zhang C, Kang H-J, Sun Y, Wang H, Naqvi A *et al.* Regulation of female reproduction by p53 and its family members. *FASEB J Off Publ Fed Am Soc Exp Biol* 2011; **25**: 2245–2255.

58 Pefani D-E, Dimaki M, Spella M, Karantzelis N, Mitsiki E, Kyrousi C *et al.* Idas, a Novel Phylogenetically Conserved Geminin-related Protein, Binds to Geminin and Is Required for Cell Cycle Progression. *J Biol Chem* 2011; **286**: 23234–23246.

59 Bao J, Li D, Wang L, Wu J, Hu Y, Wang Z *et al.* MicroRNA-449 and MicroRNA-34b/c Function Redundantly in Murine Testes by Targeting E2F Transcription Factor-Retinoblastoma Protein (E2F-pRb) Pathway. *J Biol Chem* 2012; **287**: 21686–21698.

60 Fededa JP, Esk C, Mierzwa B, Stanyte R, Yuan S, Zheng H *et al.* MicroRNA-34/449 controls mitotic spindle orientation during mammalian cortex development. *EMBO J* 2016; **35**: 2386–2398.

61 Medina-Bolívar C, González-Arnay E, Talos F, González-Gómez M, Moll UM, Meyer G. Cortical hypoplasia and ventriculomegaly of p73-deficient mice: Developmental and adult analysis: p73 in developing and adult cortex. *J Comp Neurol* 2014; **522**: 2663–2679.

62 Yang A, Walker N, Bronson R, Kaghad M, Oosterwegel M, Bonnin J *et al.* p73-deficient mice have neurological, pheromonal and inflammatory defects but lack spontaneous tumours. *Nature* 2000; **404**: 99–103.

63 Koeppel M, van Heeringen SJ, Kramer D, Smeenk L, Janssen-Megens E, Hartmann M *et al.* Crosstalk between c-Jun and TAp73alpha/beta contributes to the apoptosis-survival balance. *Nucleic Acids Res* 2011; **39**: 6069–6085.

64 Diez-Roux G, Banfi S, Sultan M, Geffers L, Anand S, Rozado D *et al.* A High-Resolution Anatomical Atlas of the Transcriptome in the Mouse Embryo. *PLoS Biol* 2011; **9**: e1000582.

Wildung et al. Figure 1

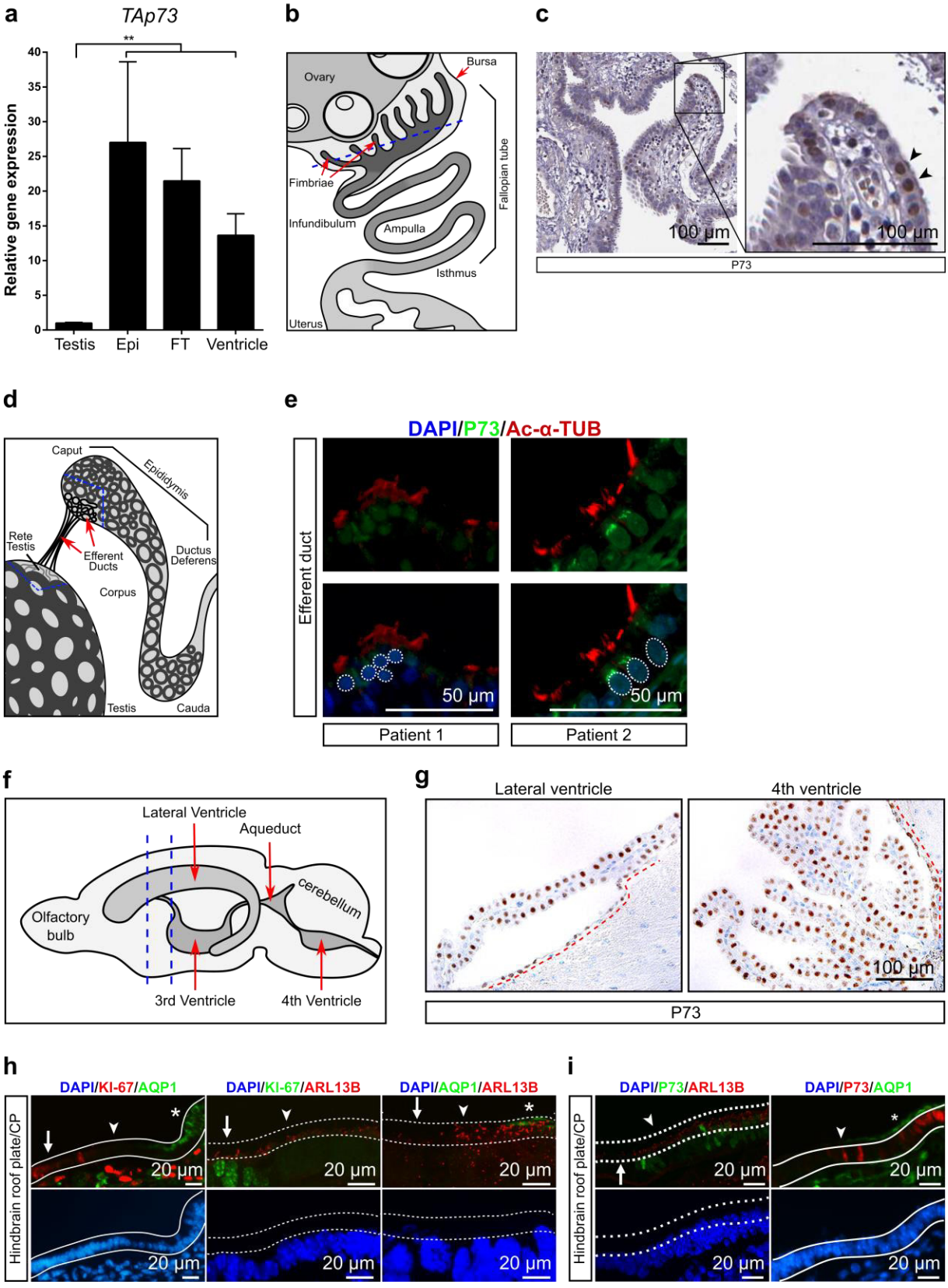

Figure 1. TAp73 is expressed in diverse multiciliated epithelial cells. (**a**) Quantitative reverse transcription PCR (RT-qPCR) analysis of *TAp73* expression in the testis, epididymis (Epi), fallopian tube (FT), and brain ventricle of wild type adult mice. Expression levels relative to *TAp73* expression in testis are shown (for testis and Epi *n*=3, for FT and ventricle *n*=4, mean ± SEM). (**b**) Schematic illustration of the fallopian tube lined by a multiciliated epithelium that connects ovary and uterus**.** (**c**) Expression of P73 is shown in the human fallopian tube. Boxed region (left) is shown in higher magnification (right) with $P73^{+}$ cells marked by arrowheads. Images were obtained from the Human Protein Atlas (https://www.proteinatlas.org/ENSG00000078900-TP73/tissue/fallopian+tube). (**d**) Schematic illustration of the multiciliated efferent ducts that connect testis and epididymis. (**e**) The expression of P73 (green) and the axonemal marker acetylated alpha tubulin (Ac-α-TUB, red) is shown in human efferent ducts. White bracket circles delineate nuclear P73 staining in merged pictures. DAPI staining (blue) marks nuclei. (**f**) Schematic illustration of the murine brain highlighting the ventricles (arrows) which are covered by MCCs. Blue dotted lines illustrate the coronal plane used for brain slices for RNA analysis. (**g**) The expression of TAp73 is shown in lateral and 4^{th} ventricles of wild type adult mice. Notice that both ependymal and choroid plexus (CP) cells express TAp73. Red dotted lines demarcate ventricles lined with ependymal cells. (**h**) The expression of KI-67, Aquaporin (AQP1, green), and ARL13B (red) in wild type hindbrain roof plate/CP at embryonic (E) day E14.5. Notice that $KI\text{-}67^{+}$ roof plate progenitors, and $AQP1^{+}$ CP epithelial cells are spatially separated. ARL13B labels monociliated roof pate progenitors and multiciliated CP epithelial cells. White lines demarcate roof pate epithelium ($KI\text{-}67^{+}/AQP1^{-}$, arrows), CP epithelium ($KI\text{-}67^{-}/AQP1^{+}$, asterisks), and "transition zone" ($KI\text{-}67^{-}/AQP1^{-}$, arrowheads) in which MCCs appear. Dotted lines mark apical surface with cilia. DAPI staining (blue) labels nuclei. (**i**) Expression of TAp73, AQP1 (green), and ARL13B (red) in wild type hindbrain roof plate/CP at day E14.5. Dotted lines mark apical surface of roof plate ($TAp73^{-}$, arrow) and transition zone ($TAp73^{+}$, arrowhead). White lines mark transition zone ($TAp73^{+}/AQP1^{-}$, arrowhead) and CP epithelium ($TAp73^{+}/AQP1^{+}$, asterisk). DAPI staining (blue) labels nuclei.

Wildung et al. Figure 2

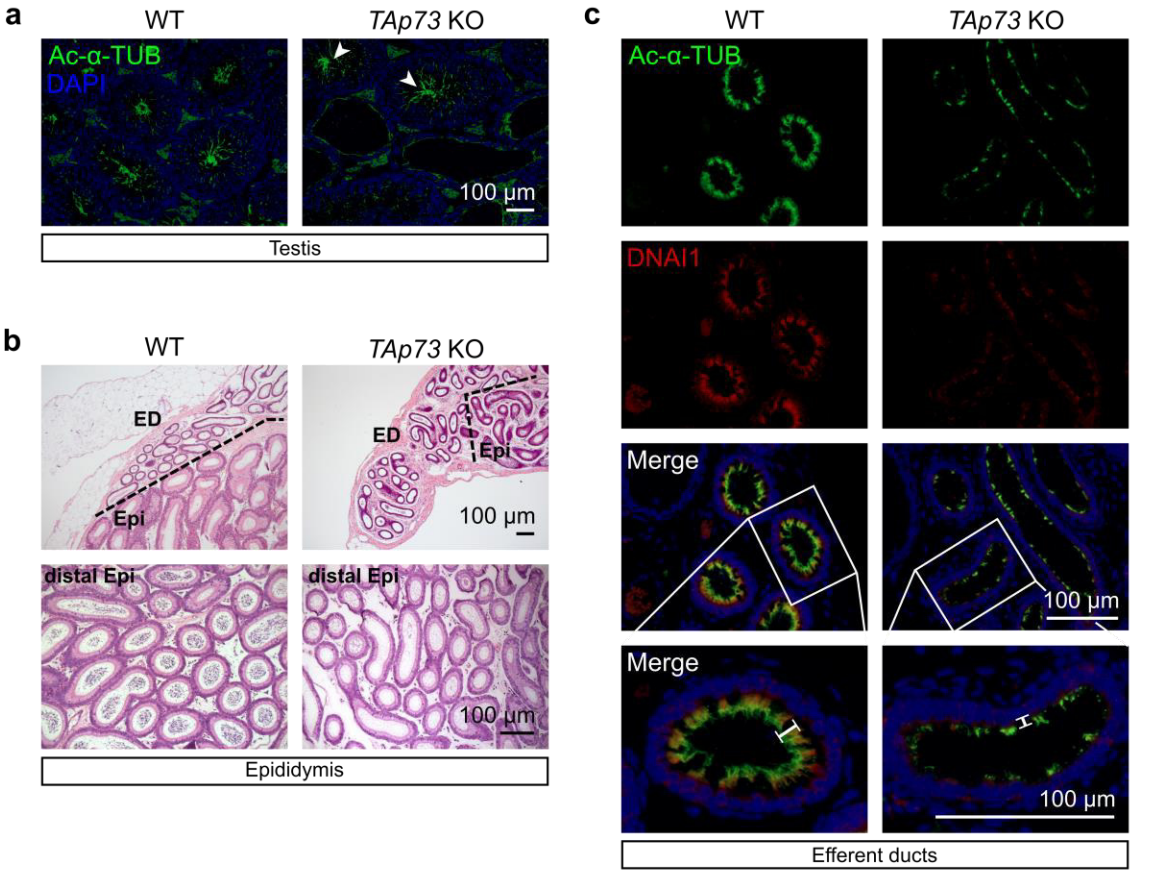

Figure 2. TAp73 controls motile multiciliogenesis in the male reproductive tract. (**a**) Representative images of the expression of Ac-α-TUB (green) are shown in testis of wild type (WT) and *TAp73* knockout (KO) mice. DAPI staining (blue) labels nuclei. Notice the presence of flagellated spermatocytes (Ac-α-TUB^{+}) in *TAp73* KO testis (arrowhead). (**b**) Representative images of hematoxylin and eosin (H&E) staining of epididymis sections in WT and *TAp73* KO animals. Bracket lines demarcate the border of efferent duct (ED) and epididymis (Epi) magnified in lower panel. Notice that *TAp73* KO mice lack mature spermatocytes in distal epididymis. (**c**) Representative images of the expression of the cilia markers Ac-α-TUB (green) and DNAI1 (red) in efferent ducts of WT and *TAp73* KO mice. DAPI staining (blue) labels nuclei. Boxed regions are magnified and illustrate reduced cilia lengths in *TAp73* KO EDs (white bars). (**d**) Quantitation of Ac-α-TUB and DNAI1 signals normalized to epithelial length shown in (**c**) (*n*=6 images from 3 WT mice; *n*=11 images from 4 *TAp73* KO mice). (**e**) Chromatin immunoprecipitation was performed for Saos2 cells transfected with TAp73α, TAp73β, and control empty vector. Binding of TAp73α (white bars) and TAp73β (black bars) to genomic regions of *FOXJ1*, *DNALI1* and *DNAI1* is compared with that of control vector (grey bars) using targeted RT-qPCR (*n*=3 for each antibody/gene pair shown, except for DNALI1 *n*=4, mean ± SEM, Genomic regions examined are illustrated in **Supplementary Figure 1** [63]). Immunoblot analysis of the expression of axonemal dyneins DNALI1 and DNAI1, TAp73, and P73 isoform lacking N-terminal (**Δ**Np73) in testis (**f**) and epididymis (**g**) of WT and *TAp73* KO animals. β-ACTIN (**f**) and Heat shock cognate 71 kDa protein (HSC70, **g**) serve as a loading control. (**h**) RT-qPCR analysis of *Dnali1, Foxj1* and *Rfx2, and Rfx3* expression in efferent ducts from WT (empty bars) and *TAp73* KO (black bars) mice (n=4 for WT (except for Rfx2 only n=3), n=3 for TAp73 KO, mean ± SEM).

Wildung et al. Figure 3

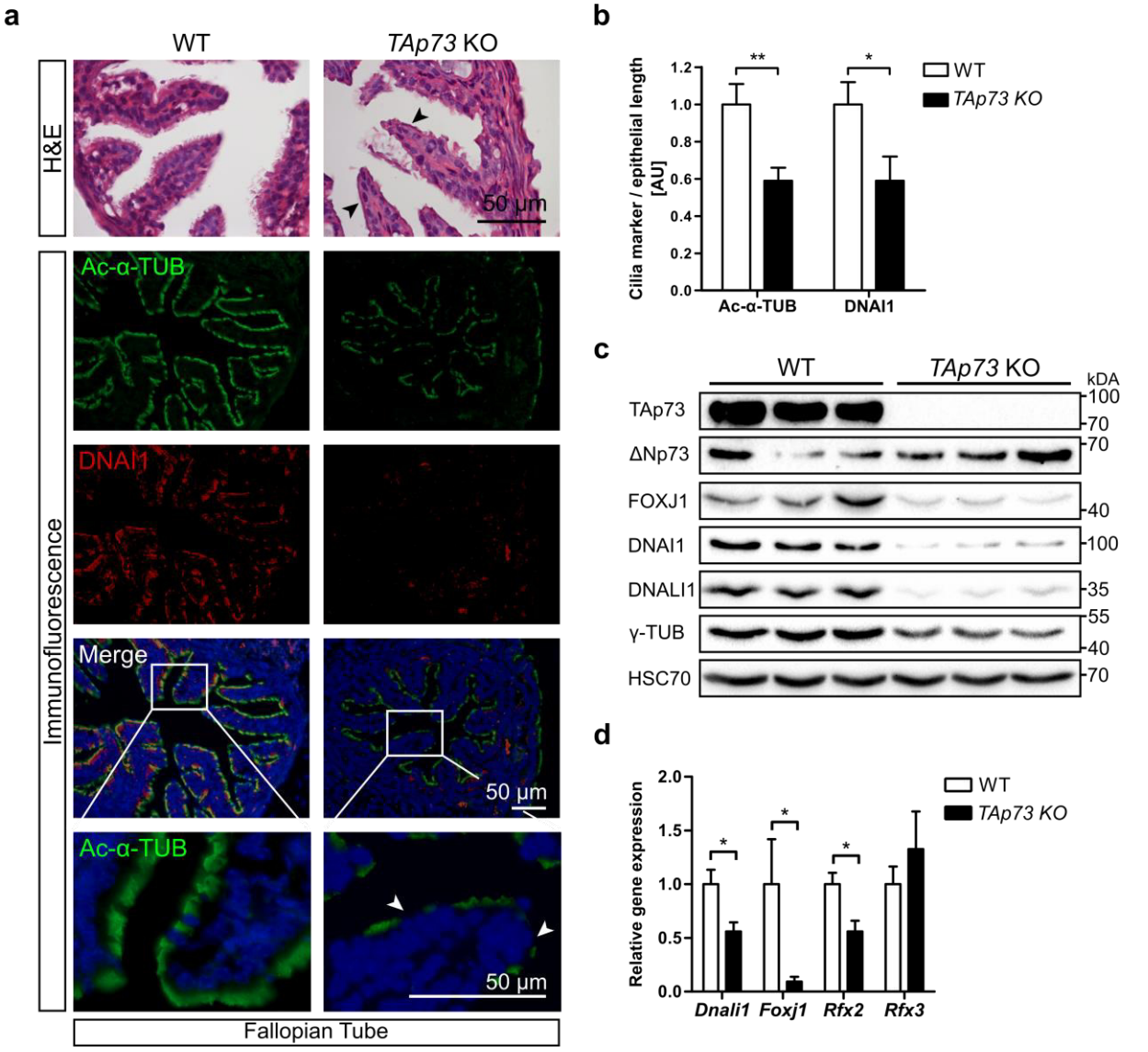

Figure 3. TAp73 controls motile multiciliogenesis in the oviducts. (**a**) Representative images of H&E staining of the fallopian tube are shown in WT and *TAp73* KO animals (upper panel). The expression of Ac-α-TUB (green) and DNAI1 (red) is shown in the fallopian tube of WT and *TAp73* KO mice (lower panels). Boxed regions are magnified and shown in the lower panel. Arrowheads illustrate non-ciliated segments of the fallopian tube of *TAp73* KO mice. DAPI staining (blue) labels nuclei. (**b**) Quantitation of Ac-α-TUB and DNAI1 signals shown in (**a**) was normalized to epithelial length (*n*=6 images from 4 WT mice; *n*=6 images from 3 *TAp73* KO mice, mean ± SEM). (**c**) Immunoblot analysis of the expression of gamma tubulin (γ-TUB), DNALI1, DNAI1, FOXJ1, TAp73, and **Δ**Np73 in oviducts from WT and *TAp73* KO animals. HSC70 serves as a loading

control. (**d**) RT-qPCR analysis of *Dnali1, Foxj1, Rfx2,* and *Rfx3* expression in oviducts from WT (empty bars) and TAp73 KO (black bars) mice (n=3 samples/genotype, mean ± SEM).

Wildung et al. Figure 4

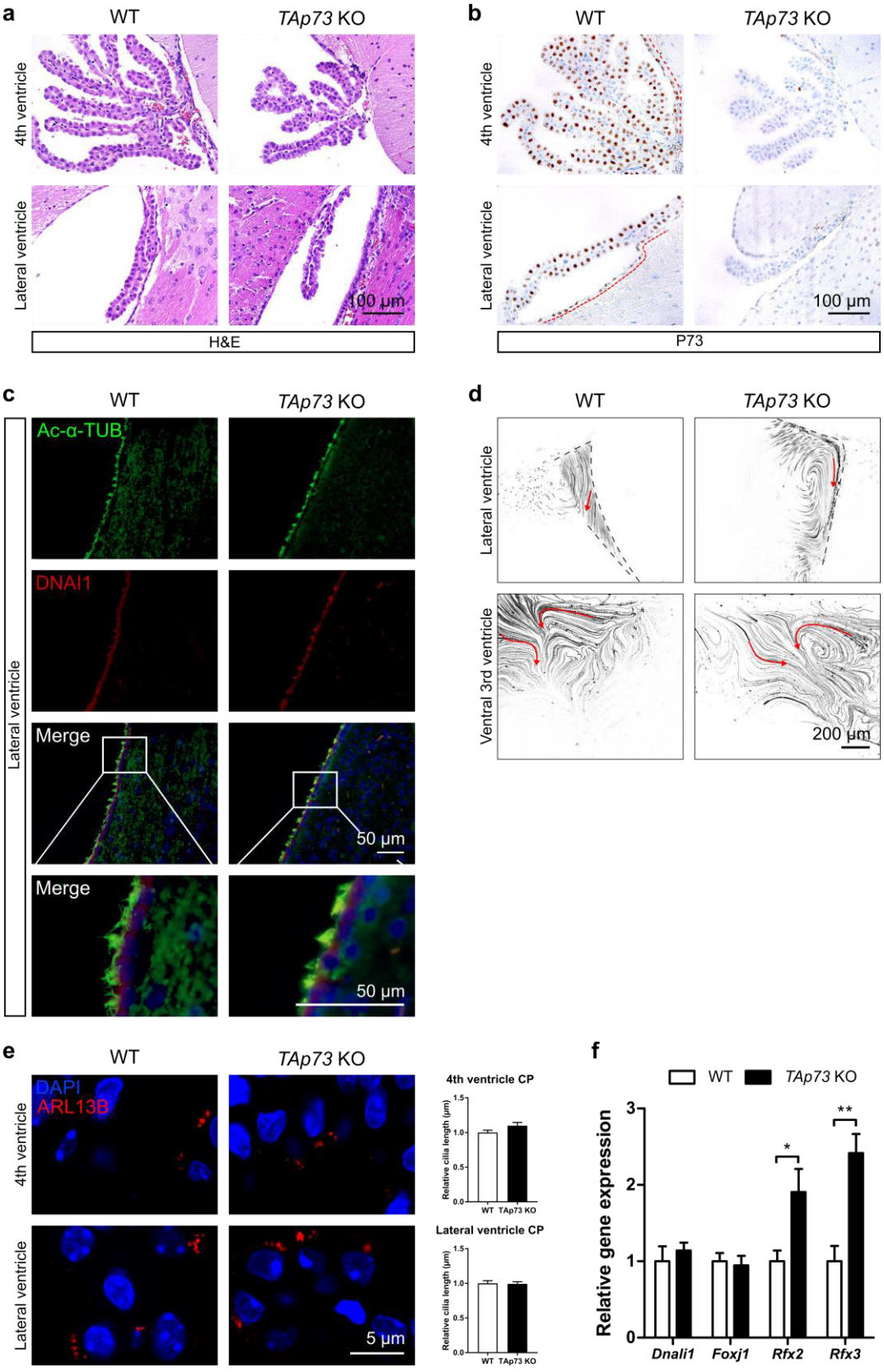

Figure 4. *TAp73* is dispensable for brain multiciliogenesis. (**a**) Representative H&E staining images are shown of ependymal and CP epithelial cells in hindbrain and lateral ventricle from WT and *TAp73* KO animals. (**b**) The expression of TAp73 is shown in ependymal and CP epithelial cells shown in (**a**). Notice that TAp73 expression is lost in these cells in *TAp73* KO mice. Red dotted lines mark ventricles lined with ependymal cells. (**c**) Representative images of the expression of Ac-α-TUB (green) and DNAI1 (red) in ependymal cells in lateral ventricle from WT and *TAp73* KO animals shown in (**a**). DAPI staining (blue) labels nuclei. Boxed regions are magnified to illustrate cilia on cell surface. (**d**) Quantitation of the movement of fluorescent beads along the ventricular system. Images of maximum intensity projections of representative movies of the lateral and the ventral 3rd ventricles are shown (*n*=3 for *TAp73*$^{-/-}$ mice; *n*=1 for TAp73$^{+/-}$ mice; and *n*=2 for WT mice). Red arrows mark the direction of bead flow. Bracket lines depict ependymal layer lining the ventricles. Refer to **Supplementary Video S3a, b** for examples of recording of ciliary beating. (**e**) The expression of the cilia marker ARL13B (red) is shown in CP epithelial cells shown in (**a**). DAPI staining (blue) labels nuclei. Graphs show quantitation of average cilia length in CP epithelial cells shown in upper and lower panels. WT *n*=2 (12 cell for 4th and 9 cells for lateral ventricle), *TAp73* KO *n*=3 (17 cell for 4th and 15 cells for lateral ventricle). (**f**) RT-qPCR analysis of *Dnali1, Foxj1, Rfx2, and Rfx3* expression in brain ventricles from WT (empty bars) and *TAp73* KO (black bars) mice (*n*=3 for WT, *n*=4 for *TAp73* KO, mean ± SEM). RNA was isolated from coronal slices with an enrichment of the lateral ventricle, blue dotted lines in **Fig. 1f** indicate the cutting area.

Wildung et al. Figure 5

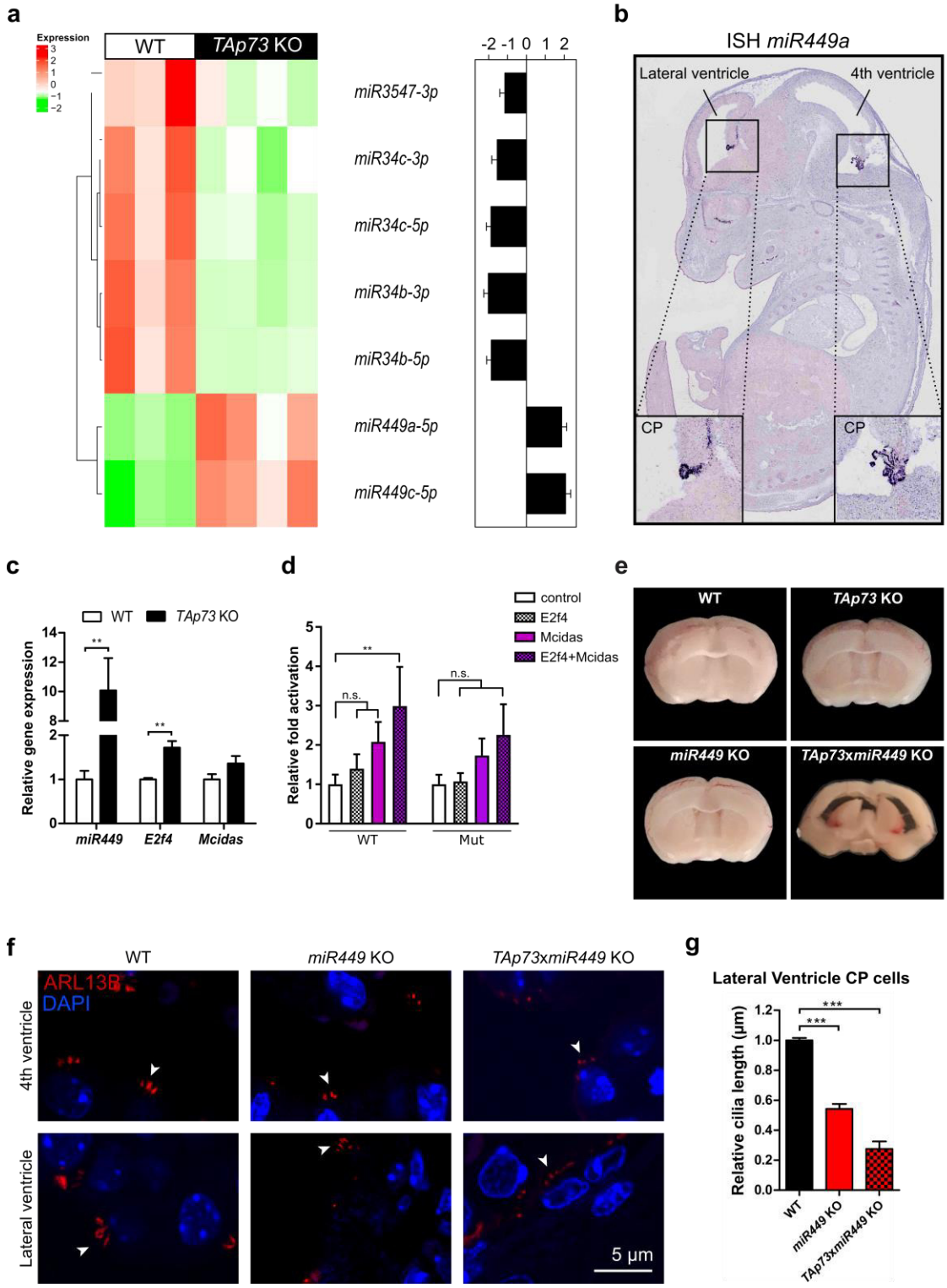

Figure 5. TAp73 functions through *miR-34/449* family in brain multiciliogenesis. (**a**) Hierarchical clustering of differentially expressed microRNAs in brain ventricles between WT and *TAp73* KO mice (left panel, *n*=3 for WT mice, n=4 for *TAp73* KO mice, mean ± SEM, one-way ANOVA, FDR < 0.05, fold change is shown). Expression differences are plotted as $\log_2$ values for microRNAs shown in heat map (right panel). Complete sRNA-seq data sets can be found in Gene Expression Omnibus (GEO) under accession number **GSE108385**. (**b**) *In situ* hybridization analysis of the expression of *miR449* in roof plate/CP at day E14.5 (http://www.eurexpress.org/ee/, [64]). (**c**) RT-qPCR analysis of *miR449*, *E2f4*, and *Mcidas* in brain ventricles from WT (empty bars) and *TAp73* KO (black bars) mice (*n*=3 for WT, *n*=4 for *TAp73* KO, mean ± SEM). (**d**) Luciferase assay of regulatory regions of *miR449* containing E2F binding motifs. *miR449* genomic sequences with three consensus E2F binding sites were identified (http://jaspar.binf.ku.dk/) and placed in front of a luciferase cassette. A deletion mutant (Mut) was created that lack the strongest consensus site but retains two milder E2F consensus sequences (**Materials and methods Table 5**). WT and Mut luciferase vectors were then co-transfected with empty vector (control, empty bars), or vectors expressing *E2F4* (checkered), *MCIDAS* (purple bars) or both (purple checkered bars). The results are shown as fold changes in luciferase activities relative to control vector (*n*=5, mean ± SEM). (**e**) Coronal brain slices as depicted by blue lines in **Fig. 1f** are shown from WT, *TAp73* KO, *miR449* KO and *TAp73/miR449* double knockout (*TAp73xmiR449* KO) mice. Note that *TAp73xmiR449* KO mice display severe hydrocephalus. (**f**) Representative images of the expression of cilia marker ARL13B (red) are shown in CP epithelial cells of hindbrain and lateral ventricles in WT, *miR449* KO, and *TAp73xmiR449* KO mice. DAPI staining (blue) labels nuclei. (**g**) Quantitation of average cilia length of CP epithelial cells shown in (**f**) (*n*=4 cells from 2 WT mice; *n*=14 cells from 4 *miR449* KO mice; n=8 cells from 4 TAp73xmiR449 KO mice, mean ± SEM).

Wildung et al. Figure 6

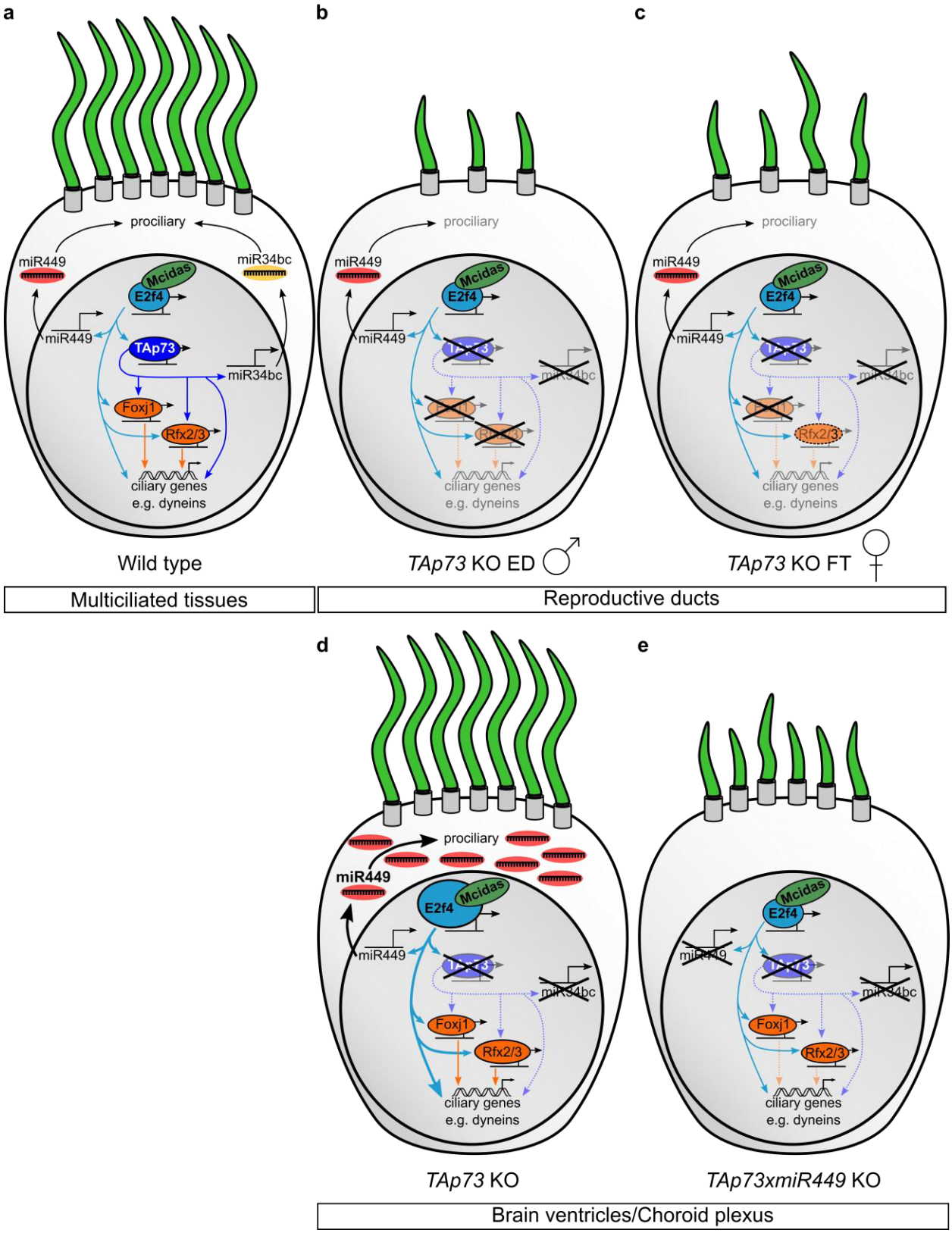

Figure 6. Schematic diagram of the molecular mechanisms of TAp73-driven multiciliogenesis in diverse tissues. (**a**) TAp73-dependent transcriptional network, including dyneins, *miR34bc*, *Foxj1, Rfx2, and Rfx3* factors, critically regulates multiciliogenesis in various ciliated tissues downstream of *E2f4*/*Mcidas*. (**b-c**) In reproductive ducts TAp73 ensures the generation of MCCs and proper gamete and zygote transport, whereas loss of *TAp73* impairs fertility in male (**b**) and female (**c**). (**d**) *TAp73* is not essential for multiciliogenesis in the brain; however, *TAp73* loss leads to upregulation of pro-ciliogenic *E2f4* and its target *miR449*. (**e**) Further removal of *miR449* in addition to *TAp73* loss leads to reduced motile cilia and severe hydrocephalus, indicating that miR449 partially compensates loss of *TAp73* in brain ciliogenesis.

Supplementary Information

MicroRNA-449 sustains cilia-related networks in the absence of transcription factor TAp73

Merit Wildung[1#], Tilman U. Esser[1#], Katie B. Grausam[2,3], Cornelia Wiedwald[1], Li Li[2], Jessica Zylla[2], Ann-Kathrin Guenther[4], Magdalena Wienken[5], Evrim Ercetin[1], Felix Bremmer[6], Orr Shomroni[7], Stefan Andreas[1], Haotian Zhao[2,3,8*] and Muriel Lizé[1,*]

 # = equal contribution; * = corresponding authors

1) **Molecular & Experimental Pneumology Group, Clinic for Cardiology and Pneumology, University Medical Center Goettingen, Germany**
2) **Cancer Biology and Immunotherapeutics Group, Sanford Research, Sioux Falls, South Dakota, USA**
3) **Division of Basic Biomedical Sciences, University of South Dakota, Sanford School of Medicine, Vermillion, South Dakota**
4) **Department of Genes and Behavior, MPI for Biophysical Chemistry, Goettingen, Germany**
5) **Institute of Molecular Oncology, University Medical Center Goettingen, Germany**
6) **Institute of Pathology, University Medical Center Goettingen, Goettingen, Germany**
7) **Microarray and Deep-Sequencing Core Facility, University Medical Center Goettingen, Germany**
8) **Department of Biomedical Sciences, New York Institute of Technology College of Osteopathic Medicine, Old Westbury, New York, USA**

Wildung et al. Supplementary Figure S1

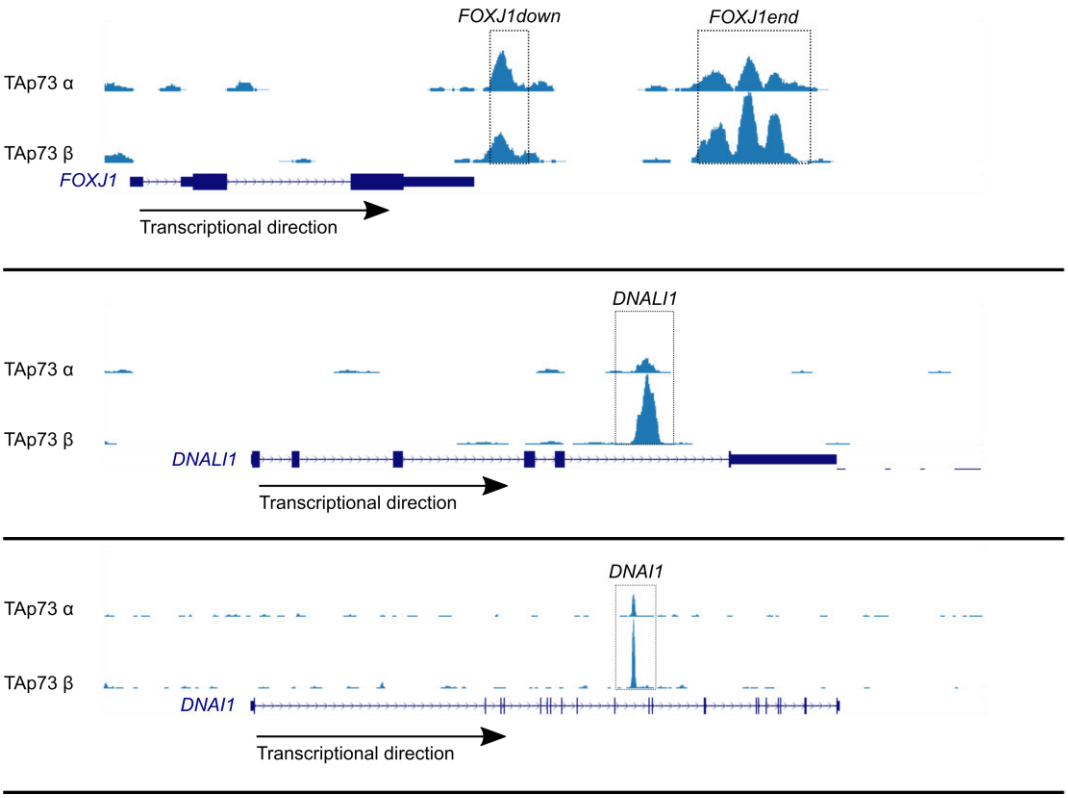

Supplementary Figure S1. TAp73 is associated with ciliary genes expressed in male and female reproductive tracts. TAp73 binding at *FOXJ1*, *DNALI1* and *DNAI1* genomic loci is shown in results from ChIPseq (Koeppel et al., 2011), Geo accession no. **GSE15780**). Boxed regions mark genomic loci enriched with TAp73 binding and validated by ChIP-qPCR in **Fig. 2e**.

Wildung et al. Supplementary Figure S2

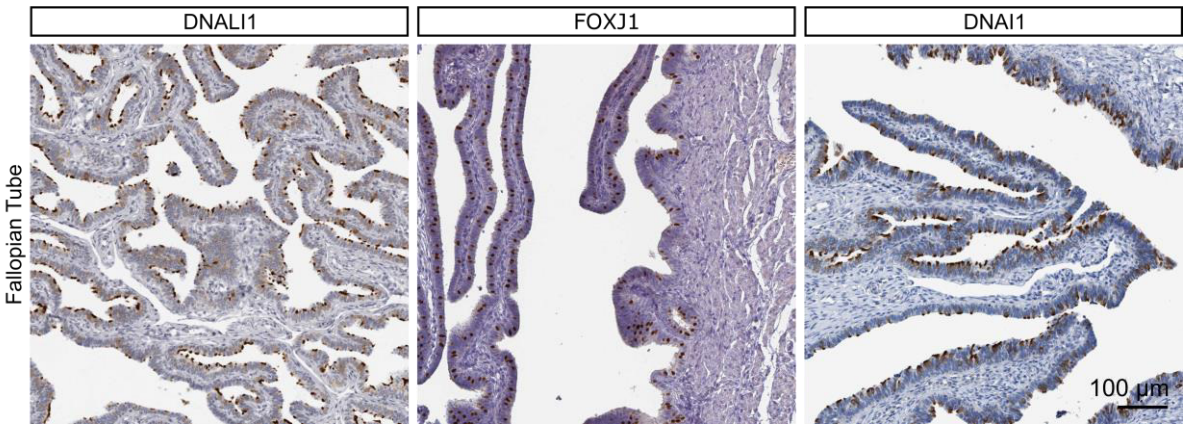

Supplementary Figure S2. Human FT epithelia express DNALI1, FOXJ1 and DNAI1. Images were retrieved from the Human Protein Atlas (DNALI1: http://www.proteinatlas.org/ENSG00000163879-DNALI1/tissue/fallopian+tube, FOXJ1: http://www.proteinatlas.org/ENSG00000129654-FOXJ1/tissue/fallopian+tube, DNAI1: http://www.proteinatlas.org/ENSG00000122735-DNAI1/tissue/fallopian+tube).

Wildung et al. Supplementary Figure S3

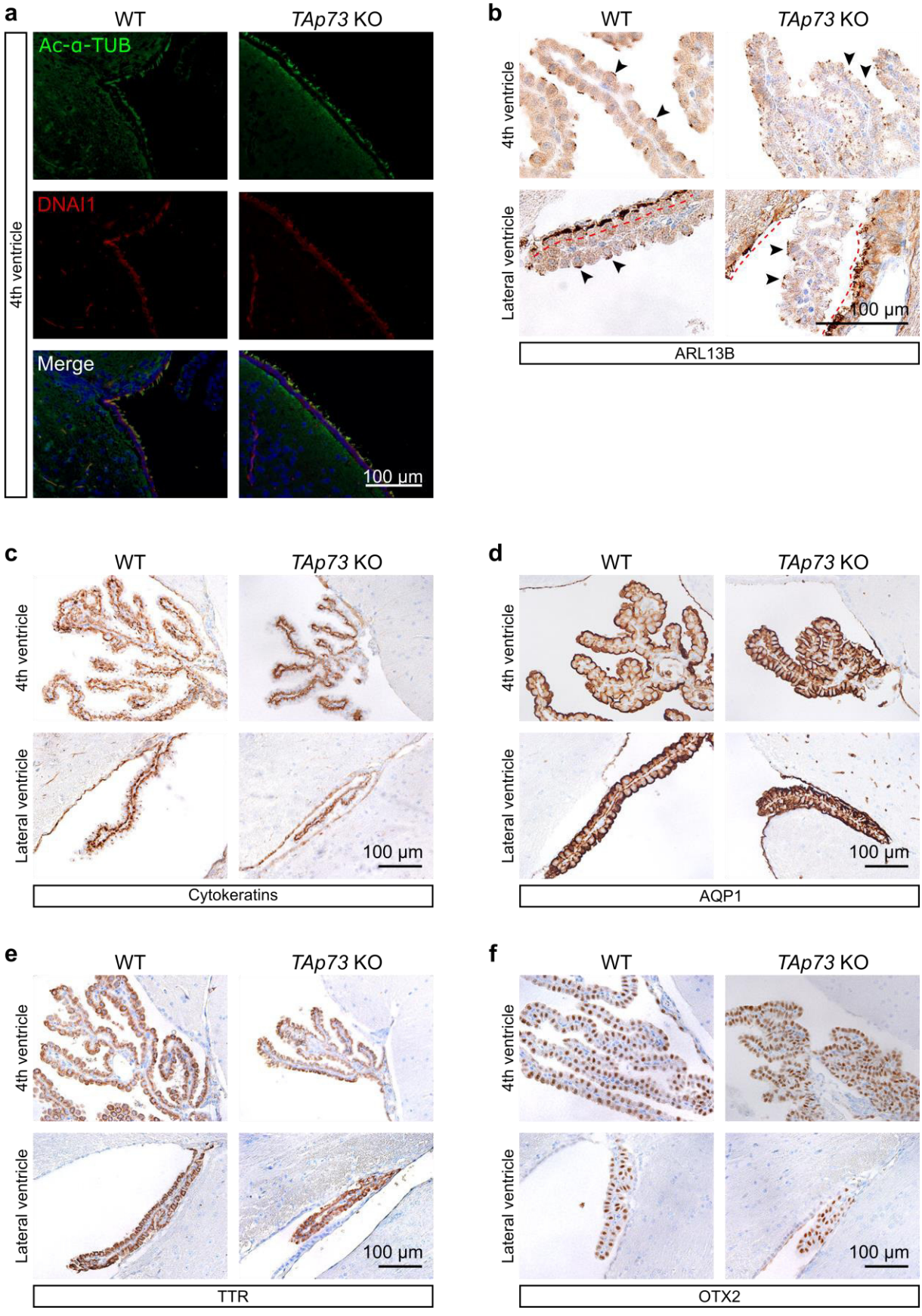

Supplementary Figure S3. *TAp73* does not obviously affect multiciliogenesis in the brain. (**a**) The expression of Ac-α-TUB (green) and DNAI1 (red) is shown in ependymal cells of the 4th ventricle from WT and *TAp73* KO animals. Representative images of the expression of ARL13B (**b,** arrowheads mark motile cilia and red dotted lines mark the boundary of lateral ventricles lined with ependymal cells), Cytokeratins (**c**), AQP1 (**d**), Transthyretin (TTR, **e**), and Orthodenticle homeobox 2 (OTX2, **f**) are shown in CP epithelium of the 4th and lateral ventricles from WT and *TAp73* KO animals.

Wildung et al. Supplementary Figure S4

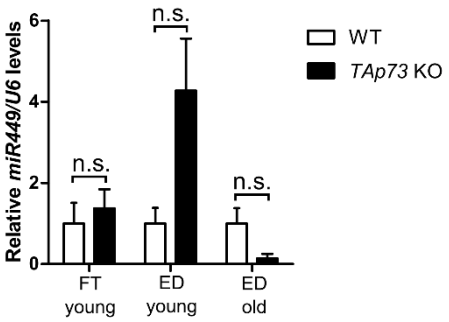

Supplementary Figure S4. FTs and EDs of *TAp73* KO do not display significant increase in *miR449* expression. Cohorts: FT young: *n*=4 samples/genotype; ED young: *n*=3 WT and *n*=5 *TAp73* KO; ED old: *n*=4 WT and *n*=3 *TAp73* KO.

Note: We cannot directly compare gene expression in "young" versus "old" ED cohorts due to age and preparation differences. However, this discrepancy fortifies the idea that, in contrast to the brain, there is no significant change in miR449 expression in response to TAp73$^{-/-}$ neither in FTs nor in EDs.

Wildung et al. Supplementary Figure S5

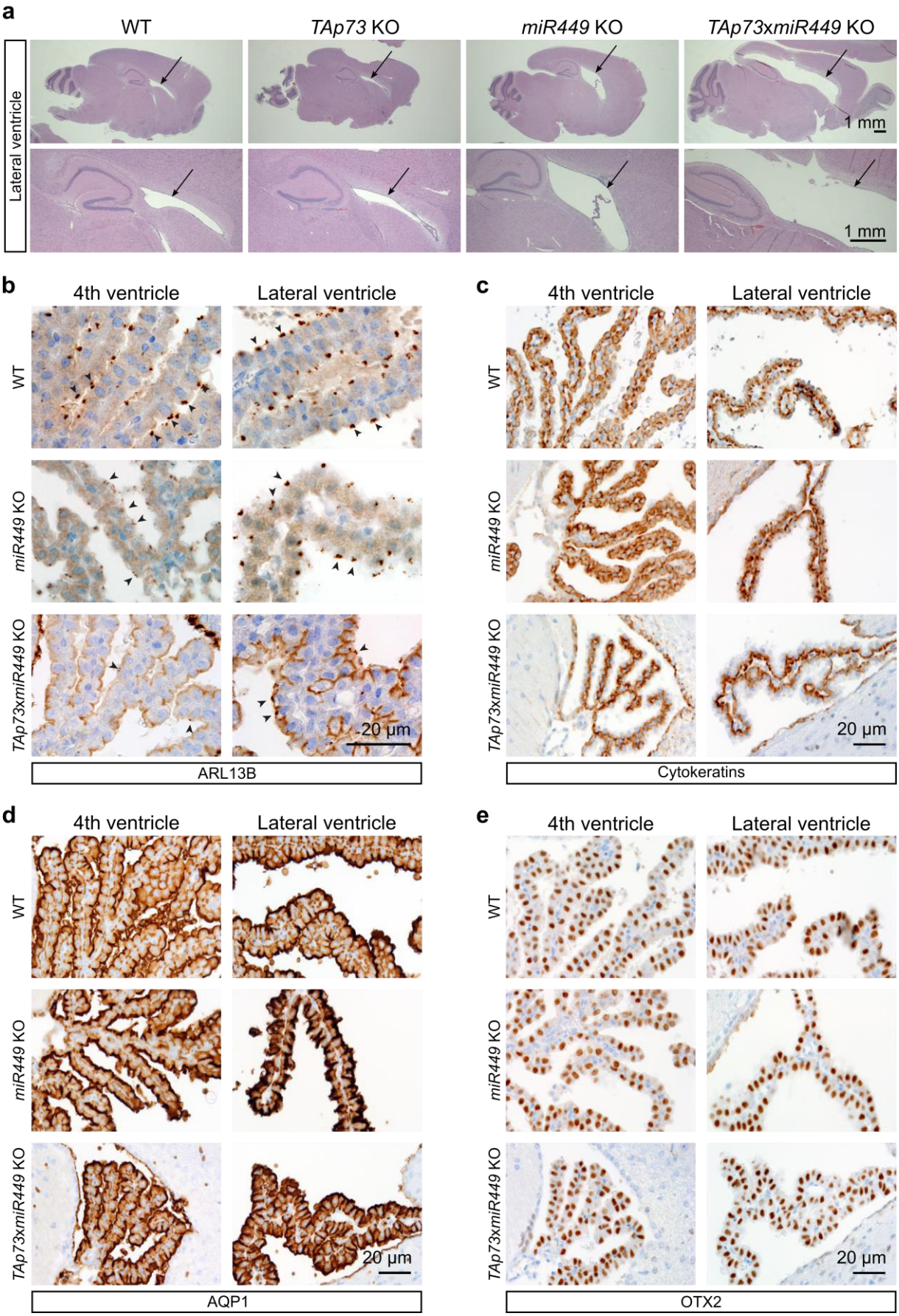

88

Supplementary Figure S5. *miR449* compensates loss of *TAp73* in brain multiciliogenesis. (**a**) Representative images of H&E staining of brain sections from WT, *TAp73* KO, *miR449* KO and *TAp73xmiR449* KO animals. Arrows point at ventricles, with *TAp73xmiR449* KO displaying a strong hydrocephalus. Representative images of the expression of ARL13B (**b,** arrowheads mark motile cilia) Cytokeratins (**c**), AQP1 (**d**), and OTX2 (**e**) in the CP epithelium of the 4th and lateral ventricles from WT, *miR449* KO, and *TAp73xmiR449* KO mice.

Wildung et al. Supplementary Figure S6

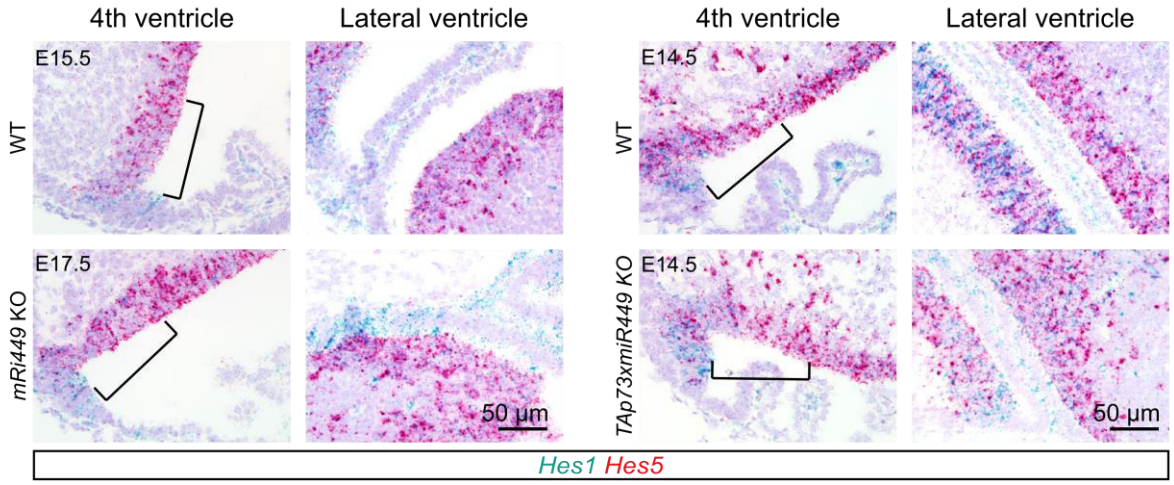

Supplementary Figure S6. NOTCH signaling is unaltered in *miR449* KO and *TAp73xmiR449* KO developing ventricles. RNAscope analysis of the expression of NOTCH targets *Hes1* (blue) and *Hes5* (red) in 4th and lateral ventricles of WT, *miR449* KO, and *TAp73xmiR449* KO mice.

Supplementary Material

Supplementary Table S1. Summary of sequencing of small RNA species from lateral ventricle/CP of WT (*n*=3) and *TAp73*$^{-/-}$ (*n*=4) mice. GEO accession number: **GSE108385.**

Supplementary Video S1. Spermatocyte movement in *TAp73*$^{+/-}$ (**a**, **b**) and *TAp73*$^{-/-}$ mice (**c**, **d**).

Supplementary Video S2. Smooth muscle contraction in fallopian tube of WT (**a**) and *TAp73*$^{-/-}$ (**b**) mice.

Supplementary Video S3. Ciliary beating in WT (**a**, 3rd ventricle) and *TAp73*$^{-/-}$ (**b**, lateral ventricle) mice.